Cement and Concrete Research 186 (2024) 107702

Contents lists available at ScienceDirect

Cement and Concrete Research

journal homepage: www.elsevier.com/locate/cemconres

Detailed characterisation of hemp and hempcrete pore structures: Effects on thermal and acoustic properties

Haemin Song [a,b], Taehwan Kim [a,*], Ailar Hajimohammadi [a], Jae Eun Oh [b], Arnaud Castel [c]

[a] Centre for Infrastructure Engineering and Safety, School of Civil and Environmental Engineering, University of New South Wales, Sydney, NSW 2052, Australia
[b] Department of Civil, Urban, Earth, and Environmental Engineering, Ulsan National Institute of Science and Technology (UNIST), UNIST-gil 50, Ulju-gun, Ulsan 44919, Republic of Korea
[c] School of Civil and Environmental Engineering, University of Technology Sydney, NSW 2007, Australia

ARTICLE INFO

Keywords:
Hempcrete
Computed tomography
3D scan
Sound absorption
Thermal conductivity

ABSTRACT

Lightweight porous composites have been widely explored to improve their acoustic and thermal performances. Hempcrete can serve as thermal insulating or soundproofing material by utilising its high porosity. However, the rigorous correlation between hempcrete thermal and acoustic performance and its pore structure remains poorly understood due to its different pore types. In this study, three hempcrete pore types [i.e., i) inter-pore between hemp and mortar, ii) hemp intra-pore, and iii) mortar intra-pore] were modified by tamping, delignification, and foaming agent conditions, respectively. Then the volumes of three types of pores were estimated using X-ray micro-computed tomography (μCT) and mercury intrusion porosimetry. The new segmentation methods were developed and their reliability and accuracy were validated. Then, the pore volumes were correlated to the thermal and acoustic properties of hempcrete. Low tamping and high delignification conditions are recommended to increase inter-pore volume and enhance hempcrete performances relating to both thermal insulation and sound absorption for real-world hempcrete applications.

1. Introduction

Hemp concrete (i.e., hempcrete) is an eco-friendly and high-performance building material that contains hemp particles in its cementitious binder. It brings some advantages to the construction industry, such as lower CO_2 emissions, lightweight, thermal insulation, and sound absorption. In recent years, hemp (*Cannabis sativa* L.) has gained popularity in the agricultural and construction sectors as a growing interest in bio-based materials derived from plants for their ability to sequester carbon during growth and their minimal environmental impact [1]. Given that hemp is composed of high porosity, hempcrete finds application as a sound-absorbing or thermally insulating material for roofs and walls [2,3] by utilising its inherent porosity to reduce sound transmission and resist heat transfer [4,5]. Moreover, compared to conventional thermal and acoustic insulation materials [6], hempcrete shows good thermal and acoustic performances as well as has a negative greenhouse gas (GHG) emission value, indicating ecological benefits from extraordinary CO_2 capture due to hemp growth and carbonation of binder [1].

Meanwhile, lightweight materials (e.g., hollow glass microsphere, wood aggregate, and entrained air) have been incorporated into cementitious material to enhance their thermal and acoustic properties by utilising their pore properties (e.g., porosity, size, and tortuosity) [7–9]. However, the quantification of different pore volumes within hempcrete is challenging for determining its thermal and acoustic properties (see Fig. 1) due to its various pore types, encompassing i) hemp intra-pores, ii) mortar intra-pores, and iii) inter-pores between hemp and mortar. Therefore, despite the significance of pore analysis of hempcrete, the majority of the research focused on the binder type, hemp size, degree of compaction, and binder contents [10–12] to improve the properties of hempcrete. In addition, most studies focused on the evaluation of the mechanical (e.g., compressive strength, hardness, bending stress, and flexural strength) [11,13] and durability properties (e.g., fire resistance, freeze-thaw resistance, salt exposure resistance, and biodegradation) [14,15] of hempcrete to apply it as a thermal insulating or sound-absorbing wall system. Not much research has been conducted on the effects of different pore types of hempcrete. Thus, the investigation of the effects of different pores will provide a thorough understanding of lightweight materials, including hempcrete.

Tamping affects the thermal and acoustic performance of hempcrete

---

* Corresponding author.
E-mail address: taehwan.kim@unsw.edu.au (T. Kim).

https://doi.org/10.1016/j.cemconres.2024.107702
Received 13 August 2024; Received in revised form 1 October 2024; Accepted 15 October 2024

through modification of its inter-pore between hemp and mortar [16]. Likewise, foaming agents can be used to change the pore structure of mortar. Foaming agents are widely used as a chemical foaming technique to develop lightweight construction materials by entrapping air void in its cementitious matrix [17,18].

Meanwhile, the delignification of hemp and the foaming agent addition to cementitious binder are applicable to modify the intra-pores of hemp and mortar, respectively. Delignification is a thermochemical treatment to remove lignin from plant cell walls, making the material easier to process for purposes like cottonizing or pulping [19,20]. For example, X. Zhao et al. did delignification to improve wood by modifying its pore structure [21]. Using appropriate delignified conditions is also important to improve the mechanical properties of hemp. In the previous studies [22–24], the strength of fibrous materials like hemp increased by alkaline treatment, but it adversely reduced in highly alkaline environments. For example, alkaline treatment made the rough surface topography and formed fibrillar, contributing to better fibre-matrix adhesion [23]. However, highly alkaline treatment removed lignin and hemicellulose, making the interfibrillar region less dense and reducing the tensile strength of the fibres [22]. When using concentrated NaOH solution, treatment times and temperatures also affect the optimum efficiency of its mechanical properties [23].

Despite the potential application of X-ray micro-computed tomography (μCT) to pore analysis of hempcrete, there is little study utilising μCT to identify different pore types in hempcrete [25–27]. This technique has emerged as a valuable tool for non-destructive image characterisation on porous materials [28]. It is widely used in cement and concrete studies, including alkali-silica reactions [29,30], cement hydration [31–33], and pore distribution and crack detection in concrete [34,35]. However, analysing different pore types in hempcrete using μCT is a challenging task due to its multiphase composition (hemp, mortar, and air voids) and different length levels of pores in hemp, hempcrete, and mortar solids as shown in Fig. 1. Moreover, hempcrete exhibits inhomogeneity due to the compressibility of hemp, contrasting with the incompressibility of other phases. Therefore, a reliable method to provide high-quality phase segmentation must be developed.

To address these challenges, this study focuses on two aspects: i) to develop a reliable segmentation method to analyse the pores in hempcrete and ii) to investigate the effects of pore modifications within hempcrete on the thermal and acoustic performance. According to the overall flowchart presented in Fig. 1, hemp intra-pores and mortar intra-pores were modified through delignification treatments and foaming agents addition, respectively, while inter-pores between hemp and mortar were modified through controlled tamping conditions using 3D-printed moulds. Material properties of raw cement were evaluated using X-ray diffraction (XRD), X-ray fluorescence (XRF), and particle size analysis. Afterwards, bulk density, thermal conductivity, and sound absorption of hemp, mortar, and hempcrete were assessed. Finally, μCT analysis was performed to explore the multiphase within hemp and hempcrete, focusing on correlating the 3D pore structures with both thermal conductivity and sound absorption characteristics of hempcrete.

2. Materials and methods

2.1. Raw materials

Hemp particles were supplied by the Australian Hemp Masonry Company (AHMC) in Australia. Australian General Purpose cement (GP cement, Boral, Australia), foaming agent (Isocem S/X, Isoltech, Italy),

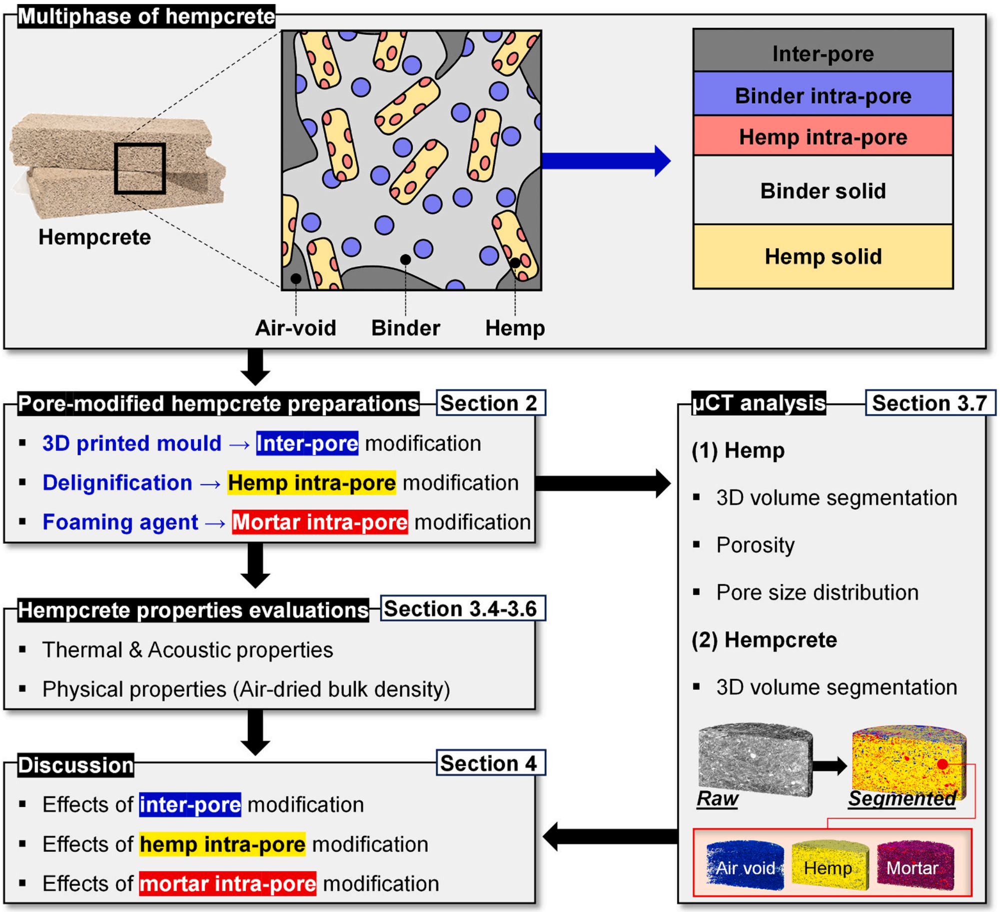

Fig. 1. Flowchart of the hempcrete pore-modification procedure.

Sydney sand (Silica sand, Australia), and analytical grade NaOH pellet (Chem-Supply, Australia) were used.

2.2. Hempcrete sample preparation with pore modifications

The present study categorised three types of pores within hempcrete: i) hemp intra-pores, ii) mortar intra-pores, and iii) inter-pores between hemp and mortar. While two types remained constant, one type was modified to assess the impact of these pores on the thermal and acoustic performances of the hempcrete. The study modified hemp intra-pore through delignification treatment, mortar intra-pore through foaming agent, and the inter-pore between hemp and mortar through controlled tamping conditions using a 3D-printed mould.

2.2.1. Intra-pore modification of hemp

Raw hemp was sieved to categorise its types and shapes. As displayed in Fig. 2, hemp exhibited significant non-uniformity in size and shape. Notably, hemp #3 (2.36–4.75 mm) and hemp #4 (1.18–2.36 mm) constituted approximately 76.2 % of the total raw hemp; thus, these sizes of hemp were exclusively used to minimise variables relating to hemp hurd type and size effects since as they affect the thermal and acoustic performance of hempcrete [16,36]. The ratio between hemp #3 and hemp #4 was approximately 1.62. A detailed summary of the sieved hemp quantities can be found in Appendix A.

One of the various delignification treatments was selected in this study to modify the hemp intra-pores. Delignification can be achieved through various methods, including enzymatic, microbial, chemical, or physical treatments [37]. For example, X. Zhao et al. [21] enhanced natural wood's thermal and acoustic properties through chemical delignification using a 5.0 wt% NaOH solution. In the present study, hemp #3 and #4 were subjected to chemical delignification to modify hemp intra-pore, following procedures in previous studies [38–40]. 3.0 *w/v*% NaOH solution was prepared by dissolving 30.0 g of NaOH pellet into 1.0 L of deionized water. Then, hemp was immersed in a 10.0 wt% hemp/NaOH solution in NaOH solution for 10 min. Subsequently, it was heated in a vacuum oven at 120 °C for either 1 or 3 h. After the treatment, hemp was washed with water and dried in an oven at 80 °C for 72 h to remove moisture. Conversely, non-delignified hemp was dried similarly without thermochemical treatment. This untreated hemp and two delignified hemps using low (1 h) and high (3 h) processes were denoted as D(0), D(L), and D(H), respectively.

2.2.2. Intra-pore modification of mortar

Besides enhancing sound absorption and thermal insulation capabilities, foaming agents have been utilised in cementitious materials to increase the mortar intra-pores [17,18]. Thus, the present study modified the intra-pore of hardened cement mortar using foaming agent additions. A compressed air foamer (DEMA, Australia) was employed to aerate the foaming agent [17], with foaming agent-to-water ratios set at 1.5 % and 3.0 %. Conditions with foaming agent-free, low foaming agent content (1.5 %), and high foaming agent content (3.0 %) were denoted as F(0), F(L), and F(H), respectively.

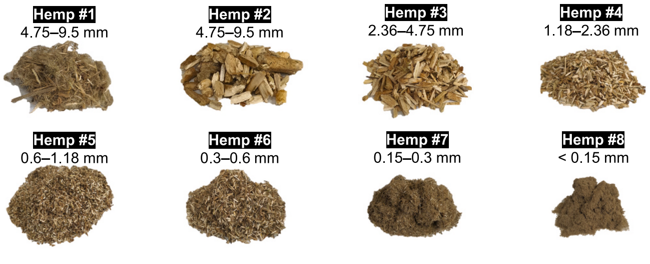

Fig. 2. Digital image of sieved hemp.

2.2.3. Inter-pore modification between hemp and mortar

Since hempcrete comprised compressible hemp and relatively incompressible phases (GP paste, sand, and water), achieving consistent tamping energy and a flat top surface for samples was challenging. To control the inter-pore between hemp and mortar, a 3D-printed mould was manufactured using the fused deposition modelling (FDM) method by a 3D printer (Ultimaker S5, Ultimaker, Netherlands). The mould consisted of an upper container, container, and bottom plate with a diameter of 99.0 mm (see Fig. 3). In particular, the diameter of the sample was specified as ϕ99.0 mm to be inserted into the impedance tube for the sound absorption test, considering the inner diameter of the tube (~100.0 mm).

After assembling those three parts, different amounts of hempcrete fresh paste (270.0, 310.0, and 340.0 g) were added to the mould and compacted to a height of 50.0 mm using a tamper. Afterwards, the upper container was removed, and the top surface was levelled using a scrapper. Samples were then covered with plastic wrap to prevent moisture evaporation, cured in a curing room, de-moulded, and stored until testing dates. Detailed curing conditions will be provided in Section 2.2.4.

Low (270.0 g), medium (310.0 g), and highly-tamped (340.0 g) conditions were denoted as T(L), T(M), and T(H), respectively. Notably, 340.0 g was the maximum weight used, as samples exceeding this weight could not be further compressed to meet the designed height (50 mm). Conversely, 270.0 g was the minimum weight utilised, as samples weighing less than this were significantly damaged during de-moulding.

2.2.4. Sample preparation

Table 1 outlines the mixture proportions for hempcrete and mortar samples. For the hempcrete sample preparations, the cement: sand: water: hemp ratio was fixed at 0.9: 0.5: 1.0: 0.5 based on the preliminary study. Hempcrete samples were prepared using different tamping conditions [T(L), T(M), T(H)] with untreated/delignified hemp [D(0), D(L), D(H)] and foaming agent additions [F(0), F(L), F(H)]. The hemp #3-to-hemp #4 ratio and bulk density of hemp and fresh mortar were considered (see Appendices A and B). The water-to-cement (w/c) ratio was maintained at 1.11, with the foaming agent-to-water ratios set at 0 %, 1.5 %, or 3.0 %. In particular, the HC-Raw sample was prepared as a reference using raw hemp without sieving or delignification. As shown in Table 1, T(M), D(0), and F(0) are omitted in the naming scheme as those were references in each modification. Thus, HC-Ref is HC-T(M)-D(0)-F(0) and, for example, HC-D(L) means HC-T(M)-D(L)-F(0), which indicates the hempcrete incorporated with the low delignified hemp, moderate tamping, and no foaming agent in mortar.

Similarly, the reference mortar sample (MO-Ref) was prepared to mirror HC-Raw proportions, except for hemp additions. Besides, other mortar samples [MO-F(0), MO-F(L), and MO-F(H)] were prepared by adjusting the w/c ratio to 0.44 to prevent severe bleeding associated with the high w/c ratio (1.11) of the MO-Ref sample.

GP cement and sand were initially mixed by hand drill with a ribbon blade for 1 min, followed by another 2 min after adding water and aerated foaming agent for mortar sample preparations. Meanwhile, hempcrete samples underwent an additional 1.5 min of mixing after the hemp addition. Fresh mortar samples were cast in 10 ml plastic tubes for the bleeding test and mercury intrusion porosimetry (MIP) analysis. Conversely, fresh hempcrete samples were cast in a 3D-printed mould (ϕ99.0 × 50.0 mm) for bulk density measurement, thermal conductivity testing, sound absorption testing, and μCT analysis. Afterwards, all samples were cured in a moist-curing room at specific temperature and humidity conditions (20.4 °C and 56.6 %, respectively) for 72 h. Following curing, the containers and bottom plates were removed, and hempcrete samples were stored under controlled conditions at 22.7 °C and 63.2 % until the testing dates.

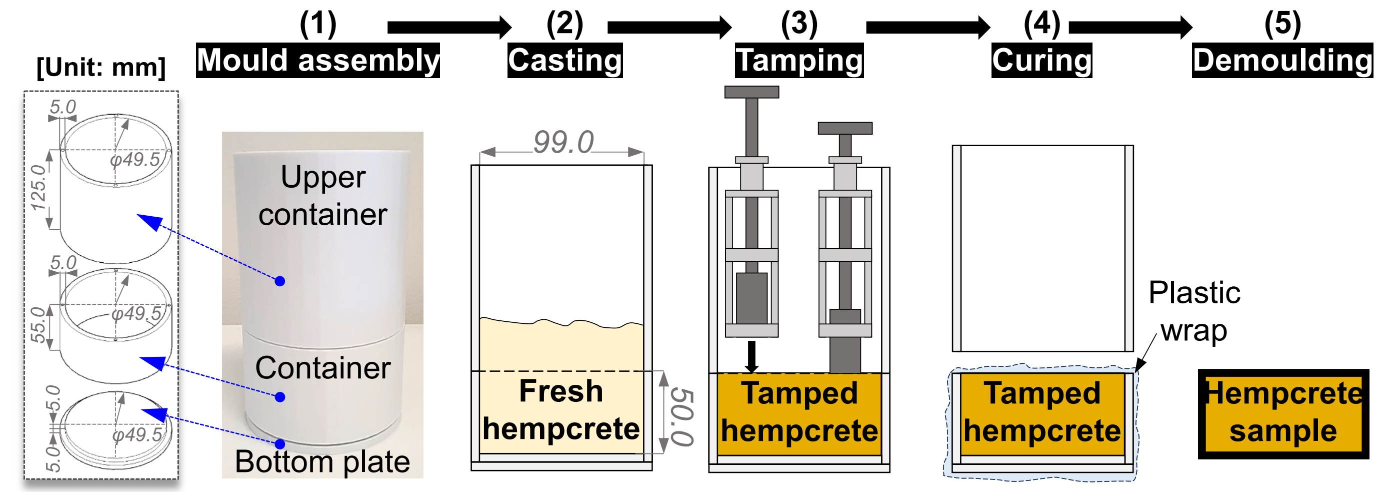

Fig. 3. Hempcrete sample preparation using a 3D-printed mould for different tamping conditions.

Table 1
Mixing proportions of mortar and hempcrete. Note: (MO) mortar, (GP) GP cement, (HC) hempcrete, (Raw) raw hemp without any treatment, (T) tamping conditions, (D) untreated/delignified hemp conditions, (F) foaming agent conditions, (0) none, (L) low, (M) medium, and (H) high.

Group	Label	Proportion (wt%)								Conditions		
		Mortar				Hemp			Sum	T	D	F
		GP	Sand	Water	Foam	Raw	#3	#4				
Hempcrete (HC)	HC-Raw	31.0	17.2	34.5	–	17.2	–	–	100.0	M	0	0
	HC-T(L)	31.0	17.2	34.5	–	–	6.6	10.7	100.0	L	0	0
	HC-Ref	31.0	17.2	34.5	–	–	6.6	10.7	100.0	M	0	0
	HC-T(H)	31.0	17.2	34.5	–	–	6.6	10.7	100.0	H	0	0
	HC-D(L)	30.7	17.1	34.1	–	–	6.8	11.3	100.0	M	L	0
	HC-D(H)	30.2	16.8	33.6	–	–	7.4	12.1	100.0	M	H	0
	HC-F(L)	29.3	16.2	32.7	0.5	–	8.1	13.2	100.0	M	0	L
	HC-F(H)	28.6	15.9	31.8	1.0	–	8.6	14.1	100.0	M	0	H
Mortar (MO)	MO-Ref	37.5	20.8	41.7	–	–	–	–	100.0	–	–	0
	MO-F(0)	50.0	27.8	22.2	–	–	–	–	100.0	–	–	0
	MO-F(L)	49.5	28.0	22.2	0.4	–	–	–	100.0	–	–	L
	MO-F(H)	49.7	27.6	22.1	0.6	–	–	–	100.0	–	–	H

2.3. *Tests on raw material and hempcrete samples*

2.3.1. *Raw material characterisation for GP cement*

The particle size distribution of the raw GP cement was analysed using a Mastesizer 2000 particle size analyser (Malvern Panalytical, United Kingdom). To assess the oxide compositions of the GP cement, X-ray fluorescence (XRF) analysis was conductedusing Axios XRF spectrometer (Malvern Panalytical, United Kingdom). X-ray diffraction (XRD) analysis was performed using PANalytical Empyrean 2 high-powder X-ray diffractometer (Malvern Panalytical, United Kingdom) with Co-Kα radiation ($\lambda = 1.79$ Å) at 2θ scanning range of 5°-60°. The International Center for Diffraction Data (ICDD) [41] was used as the reference for the XRD patterns. Then, quantitative analysis was carried out using the X'pert High Score software with Rietveld refinement.

2.3.2. *Thermogravimetric analysis (TGA) of raw hemp and treated hemp*

The thermogravimetric analyser (Q600, TA instrument, United States) was used to evaluate the compositions of an untreated hemp #3 particle and delignified particles under D(L) and D(H) conditions. Each sample, weighing 3.56 ± 0.09 mg, was placed on an alumina pan. The analysis began with an isothermal period at 30 °C for 180 min, followed by heating to 500 °C at a rate of 10 °C/min under a nitrogen (N_2) environment with a flow rate of 10 ml/min.

2.3.3. *Scanning electron microscope (SEM) of raw hemp and treated hemp*

To visually inspect the plant morphological changes due to delignification, SEM (S3400, Hitachi, Hitachi, Japan) was used to observe the internal cross-sections of untreated hemp #3 and delignified one under the D(H) condition. These hemp samples were precisely cut and affixed to the SEM holder using carbon tape. An energy level of 15 kV was employed to collect secondary images at magnifications of ×1000 and ×3000.

2.3.4. *The bulk density of mortar and hemp*

The bulk densities of mortar and hemp samples on 3, 7, and 28 days were the weight of the sample of the same volume (φ99.0×50.0 mm). Similarly, the bulk densities of hemp (raw, untreated, delignified) and fresh mortar samples [MO-F(0), MO-F(L), MO-F(H)] were measured using cylindrical containers (φ99.0×50.0 mm). Each density value was averaged from three measurements. Then, bulk densities of hardened mortar and hempcrete samples were measured at 3, 7, and 28 days. The hempcrete sample with a bulk density closest to the average of the three measurements underwent μCT analysis. Thermal conductivity and sound absorption tests were conducted on all three hempcrete samples.

2.3.5. *Mercury intrusion porosimetry of cement mortars*

The pore size distribution of cement mortar samples at 28 days was determined using a mercury intrusion porosimeter (AutoPore IV 9500, Micromeritics, United States). Hardened samples were removed from 10 ml plastic tubes and cut into 5 mm cubic pieces for the MIP test. Intrusion and extrusion were carried out within the 0.5–60,000 psi range. The penetrometer, having a bulb volume of 5 cc and a total stem volume of 1.131 cc, was used. The surface tension, contact angle, and density of mercury were 485 dyn/cm, 130°, and 13.54 g/ml, respectively.

2.3.6. Thermal conductivity

A thermal conductivity analyser (Trident, C-Therm, Canada) was employed to determine the thermal conductivity of hemp, mortar, and hempcrete samples cured at 28 days. Due to the low density and high porosity of hemp samples, their thermal conductivities were assessed using the method recommended by RILEM [42]. The flex transient plane source (TPS) probe was inserted between plastic containers (φ99.0 × 50.0 mm) filled with hemp to measure its thermal conductivity. On the other hand, a modified transient plane source (MTPS) probe was used for the mortar and hempcrete samples to measure their thermal conductivities. The probe was positioned at the bottom of the sample, and a weight of 500 g was applied on top to minimise the gap between the probe and the sample. All measurements were conducted five times, and the average value was used.

2.3.7. Sound absorption

The sound absorption coefficient (α) of hemp, mortar, and hempcrete samples was determined using a two-microphone impedance tube (B&K type 4106, Brüel & Kjær, Denmark) following the transfer function method to satisfy the ISO10534-2 standard [43]. The inner diameter of the tube was 100 mm, with a microphone separation distance of 100 mm. It should be noted that this working frequency range for the two-microphone technique depends on the diameter of the sample and the spacing between the two microphones [43]. For example, the 100 mm sample can measure up to 2000 Hz, while the 29 mm sample can measure up to 6300 Hz [44]. White noise was generated by a laptop sound speaker, amplified, and introduced into the tube to ensure uniform sound energy across all frequencies. Two microphones captured the incident sound from the speaker, and the sound reflected from the sample. The sensitivity of the two microphones was 48.19 and 46.92 mV/Pa. An analyser (NI 9234 Compact DAQ 24 bit) generated and converted the electrical signal from the data acquisition (National Instrument, United States). The captured signals were processed using MATLAB to calculate the sound absorption coefficient within the 300 to 1600 Hz frequency range based on the transfer function. Initially, the α value of the air was measured with the plunger pulled out to a depth of 20.0 cm, and the zero point was adjusted between 300 and 1600 Hz. Subsequently, after the plunger was set to a depth of 5.0 cm, hempcrete samples were inserted, and the sound absorption coefficient within the same frequency range was determined. Measurements were repeated three times, and an average value was computed.

2.3.8. X-ray micro-computed tomography (μCT)

μCT imaging was employed to determine hemp intra-porosity, pore size distribution, and the various porosities within hempcrete samples. All samples were positioned on a rotational stage and subjected to a 360° rotation. First, hemp samples were measured with a current of 185 μA and a voltage of 60 kV. The acquisition process lasted 7.5 h, and 2520 projections were obtained in a double helix mode [45]. Likewise, hempcrete samples were measured with a current of 120 μA and voltage of 80 kV. The same hempcrete samples that were tested for bulk density, thermal conductivity, and sound absorption were selected for the μCT analysis to ensure representativeness. The acquisition took 4 h, with 2880 projections acquired in circular mode. Then, the raw data were reconstructed using the Australian National Super Computing Infrastructure (NCI). The resolutions of the reconstructed tomograms for hemp and hempcrete samples were 1.748 (± 0.002) and 43.859 (± 0.005) μm/px, respectively. Following data acquisition, tomographic imaging was analysed using Aviso, a 3D visualisation software, along with ImageJ and MATLAB for further processing and analysis.

One of the key innovations in this study is the development of a systematic and reliable segmentation method for analysing the complex multiphase structure of hempcrete. This study has expended significant effort on this segmentation method, which is useful to any researcher who studies multiphase systems like hempcrete. Fig. 4 shows the whole hempcrete segmentation process using Aviso software. Raw 2D sliced images were filtered using a median filter, and noise around the sample was removed using a volume editing function. Then, the sample was divided into three parts, 7.5 mm apart from the upper and bottom surfaces, to minimise the underestimation of the air void phase in the middle part [see Fig. E1 (a)]. Next, one cubic subvolume (~6.5 mm) was extracted from each part (the upper, middle, and bottom). It should be noted that subvolumes were selected from regions that evenly contained air void, hemp, and mortar. The detailed hemp intra-pore segmentation, intra-pore size distribution of hemp, and hempcrete segmentation can be found in Appendix C, D, and E, respectively.

3. Results and analysis

3.1. Raw material analysis

Table 2 summarises the XRF, XRD, and particle size distribution results of raw GP cement. The cement composition consisted predominantly of CaO and SiO_2, with additional traces of Al_2O_3, Fe_2O_3, and SO_3. XRD analysis revealed the presence of various compounds, including C_3S, C_2S, C_3A, C_4AF, $CaCO_3$, and $CaSO_4{\cdot}2H_2O$. Its median particle size (D_{50}) was determined to be 16.97 μm. A previous study of the authors determined the properties of the Sydney sand used in this study [46]. The specific gravity, water absorption, and D_{50} of the sand are 2.65, 3.50 %, and 0.35 mm, respectively.

3.2. Intra-pore modification of hemp through delignification

Fig. 5 illustrates the differential thermogravimetric (DTG) curves of untreated hemp #3 and delignified ones [D(L) and D(H) conditions]. Cellulose was thermally decomposed at 250–350 °C due to the thermal decomposition of its molecular structures, and lignin was thermally decomposed at 150–450 °C due to the degradation of guaiacyl and syringyl compounds [38]. Delignification resulted in decreased amounts of cellulose compared to untreated hemp #3; consequently, delignification modified the hemp composition.

Fig. 6 presents the SEM secondary images of untreated hemp #3 and delignified one under the D(H) condition. While they exhibited uneven plant cell walls [see Fig. 6 (a) and (c)], the untreated hemp had uniform plant cell sizes, whereas delignified hemp had irregular sizes. Furthermore, Fig. 6 (b) displays well-connected plant cells in untreated hemp, whereas Fig. 6 (d) shows partially disconnected and perforated cells in delignified hemp. Hence, delignification appeared to modify the morphology of the intra-pore structure of hemp.

3.3. Intra-pore modification of mortar through foaming agent

Fig. 7 visually examines the cement mortar samples with foaming agent additions. The MO-Ref sample showed severe bleeding due to its high w/c ratio of 1.11, the same w/c ratio used for the HC-Ref sample. Hempcrete required more water than conventional concretes or mortars because it contains a high volume of hemp with significant porosity, leading to substantial water absorption (see Fig. 6). Insufficient water would result in absorption by the hemp instead of enabling cement hydration. To address this issue, the study adjusted the w/c ratio to 0.44 (i.e., 4.0/9.0) to minimise the bleeding, based on the preliminary test and previous studies, which recommended w/c ratio range of 0.35–0.57 for the foamed concrete [47,48].

Fig. 8 illustrates the bulk density of mortar samples by adding a foaming agent. The initial bulk densities of fresh MO-F(0), MO-F(L), and MO-F(H) samples were 1955.2 (± 0.0), 1509.7 (± 0.0), and 1386.5 (± 0.0) kg/m^3, respectively. Adding foaming agents reduced the bulk density by 22.8–29.1 % compared to the mortar sample without foaming

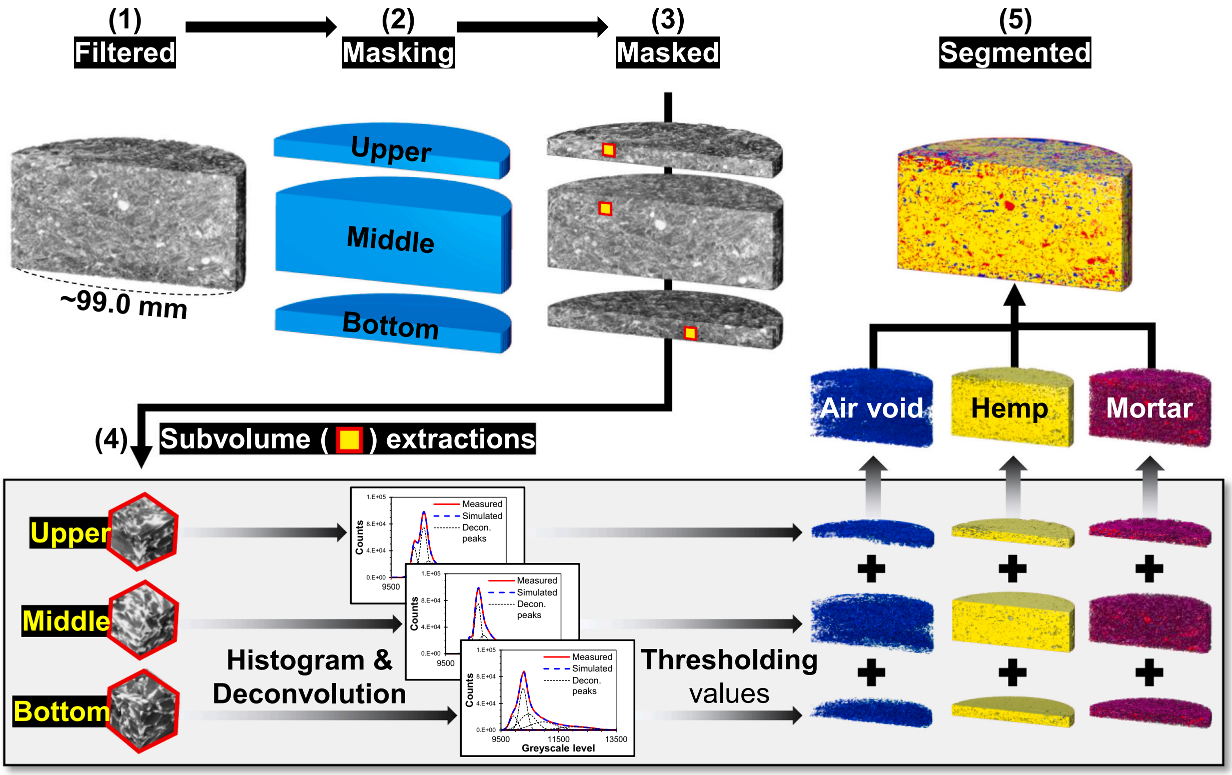

Fig. 4. Hempcrete segmenting process using Aviso software.

Table 2
Raw material result of GP cement.

Oxides (wt%)		Compounds (wt%)		Size (μm)	
CaO	64.86	Tricalcium silicate, C_3S	58.6	D_{10}	3.28
SiO_2	19.37	Dicalcium silicate, C_2S	24.4	D_{50}	16.97
Al_2O_3	4.50	Tricalcium aluminate, C_3A	6.0	D_{90}	41.82
Fe_2O_3	2.95	Calcite, $CaCO_3$	4.4		
SO_3	2.07	Tetracalcium aluminoferrite, C_4AF	4.1		
Loss on ignition	5.24	Gypsum, $CaSO_4•2H_2O$	2.6		

agents (i.e., MO-F(0)). Their bulk densities at 28 days were measured at 1892.9 (± 54.9), 1456.1 (± 31.3), and 1333.0 (± 20.1) kg/m^3, respectively. Consequently, only slight reductions of 3.2–3.9 % in bulk density were observed after 28 days of curing.

Fig. 9 displays the pore size distributions of mortar samples as measured by a mercury intrusion porosimeter. However, the MIP method cannot accurately represent absolute porosity across all pore sizes due to its intrinsic limitation. The ink-bottle effect is a well-known phenomenon that causes the overestimation of small pores, and high pressure applied to the sample can damage its microstructure [49–51]. Thus, the pore size distribution obtained from MIP (shown in Fig. 9) is not the actual pore size distribution but the threshold diameter of the pore entrance [50,51]. However, given that A. Vishavkarma [52] reported that most pore sizes of foamed concrete ranged from 10 to 200 μm, the mercury intrudable pore volume (3 nm to 300 μm) can still be valid for comparing relative pore volumes of mortars with different foaming agent additions.

The pore volume within the range from 3 nm to 300 μm of MO-F(0), MO-F(L), and MO-F(H) was 23.2 %, 35.7 %, and 44.3 %, respectively. Foaming agent additions notably increased the presence of pores larger than approximately 1.0 μm. This indicates that foaming agent additions modified the intra-pore structure of mortar.

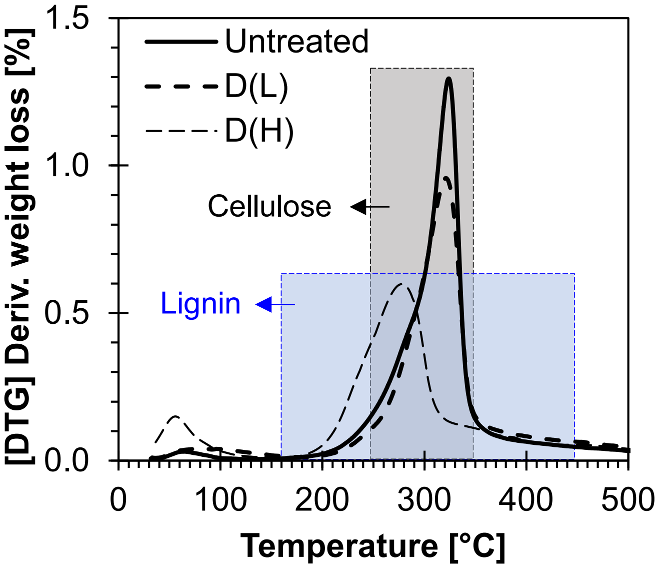

Fig. 5. DTG results of untreated hemp #3 and delignified ones under D(L) and D(H) conditions.

3.4. *Inter-pore modification between hemp and mortar through controlled tamping condition*

Fig. 10 illustrates the bulk density of hempcrete samples. Specifically, the HC-T(L), HC-T(M), and HC-T(H) samples exhibited fresh paste densities of 701.8, 805.8, and 883.8 kg/m^3, respectively. Notably, hempcrete samples exhibited significant differences in bulk density depending on the tamping conditions. Their bulk densities at 28 days were 600.4, 714.0, and 768.7 kg/m^3, respectively, indicating a reduction in bulk density of 11.4–14.4 % due to water loss during curing.

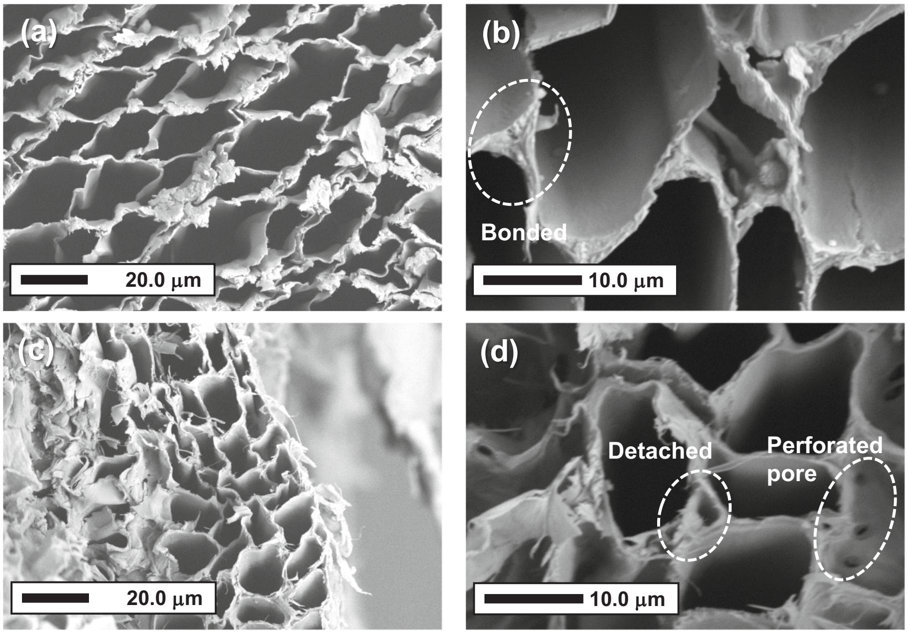

Fig. 6. Cross-sectional SEM images of hemp #3 particle: untreated one at (a) × 1000 and (b) × 3000 and delignified one under D(H) condition at (c) × 1000 and (d) × 3000.

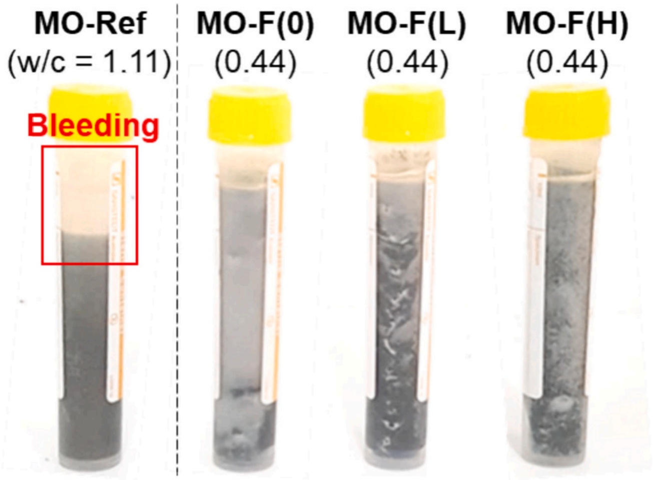

Fig. 7. Visual inspection for bleeding of mortar samples.

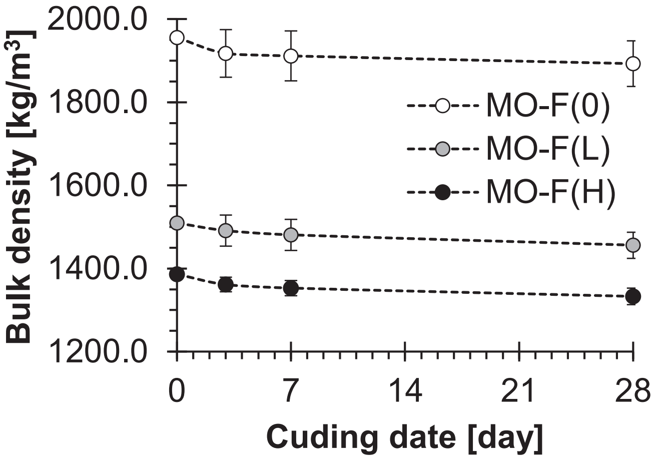

Fig. 8. Bulk density of mortar samples.

Likewise, other samples [HC-Raw, HC-D(L), HC-D(H), HC-F(L), HC-F(H)] exhibited the same fresh bulk density of 805.8 kg/m^3 as the exact same mass of each mixture was compacted to the same volume of mould. Their bulk densities at 28 days (approximately 665.3–684.7 kg/m^3) were slightly lower or comparable to that of HC-Ref (714.0 kg/m^3). Samples also experienced 10.7 to 17.4 % bulk density reduction due to water loss during the curing period. Thus, hempcrete sample properties were time-dependent due to hemp additions because of the more significant bulk density changes over the curing period compared to mortar samples (3.2–3.9 % in Fig. 8).

3.5. Thermal conductivity

Fig. 11 depicts the thermal conductivity of hemp, mortar, and hempcrete samples at 28 days. Fig. 11 (a) shows that raw hemp had a thermal conductivity of 87.2 mW/m·K. After drying at 80 °C for 72 h, the thermal conductivities of hemp #3 and hemp #4 decreased to 78.6 and 75.3 mW/m·K, respectively, reflecting a reduction of 9.9 to 13.8 %. Then, delignification further lowered their thermal conductivity, with reductions of 1.5–7.0 % under D(L) and 10.0–23.9 % under D(H) conditions.

In Fig. 11 (b), mortar samples exhibited higher thermal conductivity than hemp samples regardless of foaming agent additions. Compared to the mortar sample without foaming agent, foaming agent additions led to thermal conductivity reductions of 25.4 % for F(L) and 34.6 % for F(H) conditions.

In contrast, hempcrete samples in Fig. 11 (c) had thermal conductivities ranging from 69.0 to 150.0 mW/m·K, closer to those of hemp samples (59.8–87.2 mW/m·K) than those of mortar samples (948.3–1450.7 mW/m·K). The standard deviations of the thermal conductivity for HC-Raw and HC-T(H) were 30.7 and 21.9 mW/m·K, respectively, while those for other samples were lower than 8.8 mW/m·K.

Meanwhile, tamping significantly increased the thermal conductivity of the hempcrete samples, while delignification and foaming agents had a lesser impact on reducing it. For example, the thermal conductivity increased by 67.8 % when comparing HC-T(L) with HC-T(M). On

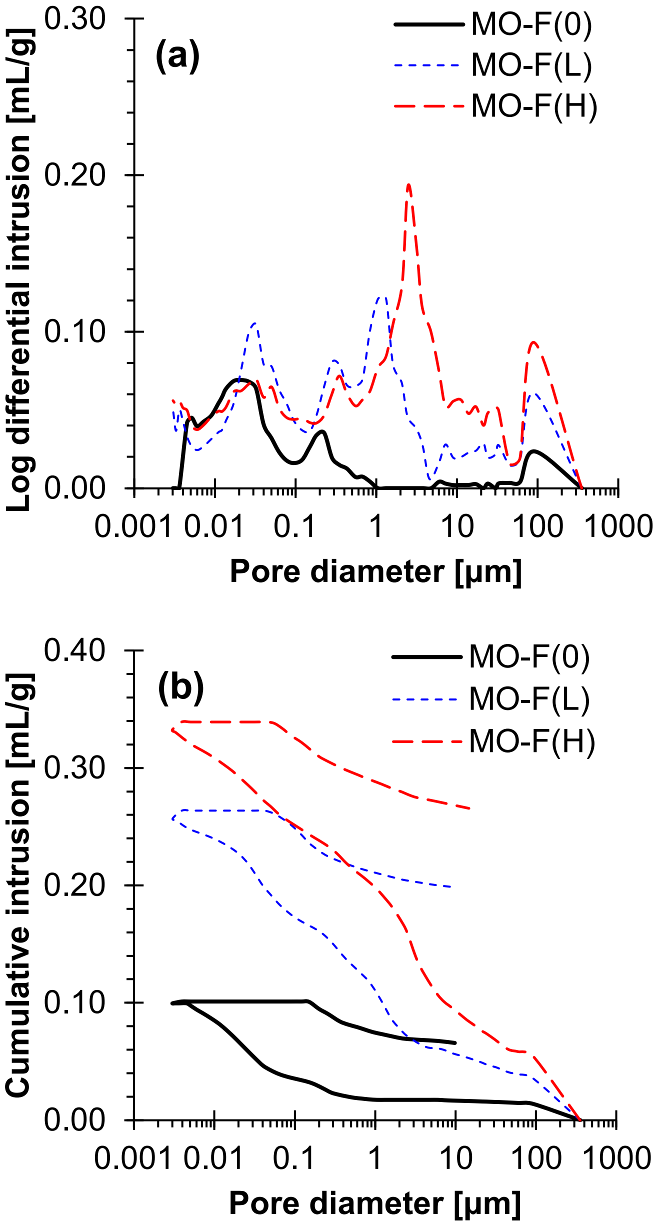

Fig. 9. Pore size distribution of mortar samples cured at 28 days.

the other hand, compared to the HC-T(M)-D(0)-H(0) sample, delignification reduced the thermal conductivity by 29.0 % under D(L) and 32.0 % under D(H) conditions. Similarly, foaming agent additions reduced the thermal conductivity by only 6.8 % under F(L) and 12.3 % under F (H) conditions. On the other hand, the delignification of hemp and the foaming of mortar enhance the thermal resistance of hempcrete. Compared to the HC-Raw sample, the HC-Ref sample exhibited a 32.3 % reduction in thermal conductivity due to the use of sieved and dried hemp with lower moisture content. The correlation between thermal conductivities and the pores of hempcrete will be further discussed in Section 4.1.

3.6. Sound absorption coefficient

While the human hearing range is 16 to 20,000 Hz, the ear is most sensitive at about 200 to 10,000 Hz, representing the range primarily used for communication [53]. In this study, as shown in Fig. 12, the sound impedance tube could only provide the sound absorption coefficient (α) of hemp, mortar, and hempcrete samples between the frequency range 300 to 1600 Hz. As mentioned in Section 2.3.7, the working frequency range monitored is a function of the diameter and the spacing between the microphones. The current study used a two-microphone impedance tube with a diameter of 100 mm and a working frequency range of 300 to 1600 Hz.

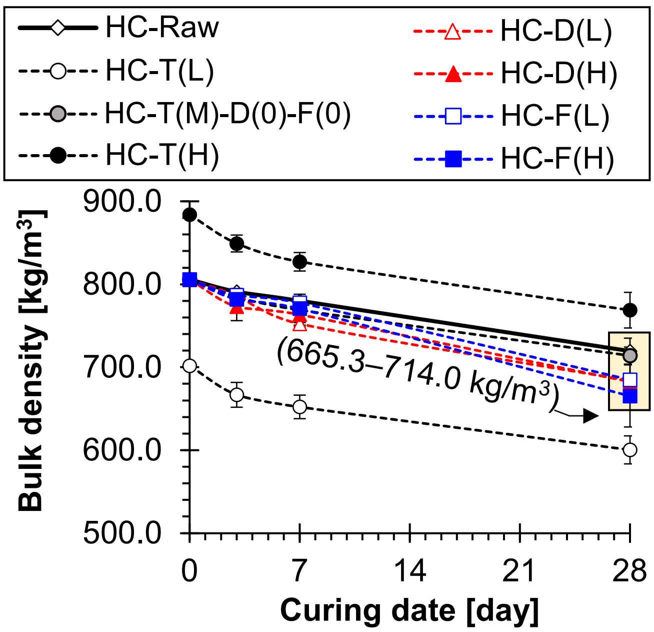

Fig. 10. Density changes of all hempcrete samples.

In Fig. 12 (a), all hemp had maximum α values at 0.84–0.90 between 1200 and 1400 Hz. In particular, raw hemp exhibited slightly higher sound absorption than hemp #3 and #4.

The foaming agent additions [see Fig. 12 (b)] increased the sound absorption within the 400–1200 Hz range but decreased it between 1200 and 1400 Hz, shifting the maximum absorption from 1400 Hz to 1000 Hz. In particular, there was almost no difference between F(L) and F(H) conditions.

Fig. 12 (c–e) shows the influence of tamping, delignification, and foaming agent conditions on the sound absorption of hempcrete samples. All hempcrete samples showed a maximum sound absorption at 600 Hz. Fig. 12 (c) illustrates that high tamping conditions significantly reduced the sound absorption of hempcrete, lowering the maximum sound absorption coefficient (α) at 600 Hz from 0.75 to 0.47. Conversely, high delignification conditions increased the maximum α value to 0.55–0.70 [see Fig. 12 (d)], while high foaming agent conditions raised it to 0.55–0.63 [see Fig. 12 (e)]. Remarkably, minimal disparity was observed between HC-F(L) and HC-F(H), which was consistent with the trends observed in hardened mortar samples [see Fig. 12 (b)]. Their sound absorption coefficient will be compared with three different types of pores within hempcrete in Section 4.1.

3.7. Microstructure of hemp and hempcrete obtained from μCT

3.7.1. Hemp segmentation

Fig. 13 presents 3D images and 2D sliced imagess before and after segmentation. Hemp solid (yellow; plant cell wall) and hemp intra-pore (black) were segmented using the Otsu thresholding mode because it identified the solid and intra-pore phases of hemp (see Appendix C). In particular, the 2D sliced image in X-Y view showed that hemp was composed of widely distributed pores of about 10 μm, with a few pores larger than 30 μm. It was consistent with the cross-sectional images collected by SEM (see Fig. 6). It should be noted that untreated hemp #3 showed high porosity (69.5 %), consistent with the previous studies reporting the intra-porosity of hemp as 42.6–82.5 % depending on the

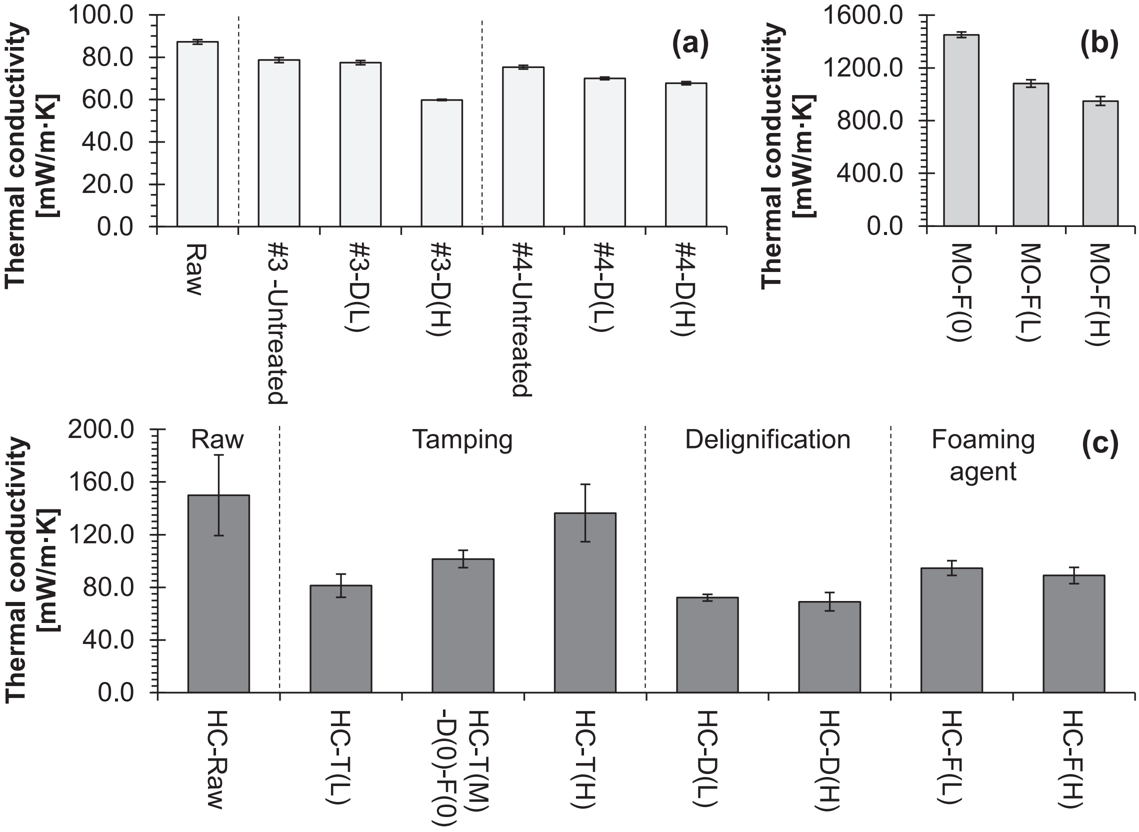

Fig. 11. Thermal conductivity of (a) hemp, (b) mortar, and (c) hempcrete samples.

hemp sources [16,54]. However, delignification gradually decreased the porosity of hemp. For instance, delignified hemp under the D(L) condition showed a porosity of 62.1 %, while that under the D(H) condition exhibited a porosity of 59.7 %.

The hemp intra-pore was shaped like cylinders because it should supply water vertically from the roots to the leaves (see Fig. D1). Unfortunately, although the Avizo 3D visualisation software enabled the measurement of sphere diameter, it could not provide that of cylinder diameter. Thus, in this study, a cylindrical pore model was suggested to compute the intra-pore diameter of hemp, which assumed that the shape of the intra-pores can be described as a cylinder. The detailed cylindrical pore model and its validation are in Appendix D.

Since this model assumed the intra-pore structure of hemp as a cylinder, there might be potential differences between the calculated and actual pore diameter values. Nevertheless, this method was helpful in the relative analysis of irregular structures close to cylinders that Aviso could not calculate. For instance, Fig. 14 displays the intra-pore size (cylinder diameter) distribution of hemp with different delignification conditions. The intra-pore size of hemp ranged from 2 to 30 μm. Notably, delignification led to a reduction in pores smaller than 8 μm and an increase in pores sized between 8 and 14 μm. These pore size changes indicated the disappearance of small pores, which merged into larger ones following the delignification treatment.

3.7.2. *Hempcrete segmentation*

Due to resolution limitations (43.859 ± 0.005 μm/px), the intra-pore within hemp and mortar could not be segmented. Instead, as shown in Fig. 15 (a), the present study segmented hempcrete into three phases: i) air void phase (inter-pore between hemp and mortar), ii) hemp phase including its solid and intra-pore, and iii) mortar phase including its solid and intra-pore. Two thresholding values were systematically determined to determine the air void-to-hemp and hemp-to-mortar boundaries. These thresholding values were computed through the deconvolution of their colour map histograms obtained from the extracted sub-volumes based on similar approaches from the literature [55,56]. To the best of the authors' knowledge, a systematic segmentation method to analyse the complex hempcrete system is first introduced in this paper, and further details and validation of the hempcrete segmentation process can be found in Appendix E.

For example, Fig. 15 (c) displays the segmented 2D slice of the HC-Ref sample with three following phases: air void (blue), hemp (yellow), and mortar (red). Although some areas of the three phases were not segmented ideally, the overall image segmentation was highly satisfactory, given that hempcrete segmentation was challenging due to its multiphase composition, inhomogeneity, and time dependency. This study attempted to minimise these difficulties by using a 3D-printed mould to apply the same degree of compaction, sieving hemp to minimise the variety of hemp sizes and shapes, and curing all specimens under the same controlled environment. However, it should be noted that there are still limitations in the μCT segmentation for hempcrete. For example, the intra-pores of the hemp and mortar could not be segmented due to insufficient resolution, but these pores might be analysed in future studies by reducing the sample size to improve the resolution.

Fig. 16 shows the volume fractions of the three phases in hempcrete samples to compare the phase changes regarding different pore modification conditions. Detailed 2D tomograms for segmented hempcrete under different pore-modifying conditions can be found in Fig. E3. High tamping conditions notably increased the mortar volume fraction while reducing air void and hemp fractions. Notably, the air void fraction in the HC-T(H) sample was nearly negligible, approximately 1.3 %. Samples with delignified hemp [HC-D(L) and HC-D(H)] seem to have volume fractions similar to the ones in the reference sample (HC-Ref). Foaming agent additions resulted in a slight increase in the air void fraction by +2.5%pt. (point percentage) and the hemp fraction by +3.5%pt., along with a decrease in the mortar fraction by −6.1%pt. compared to the

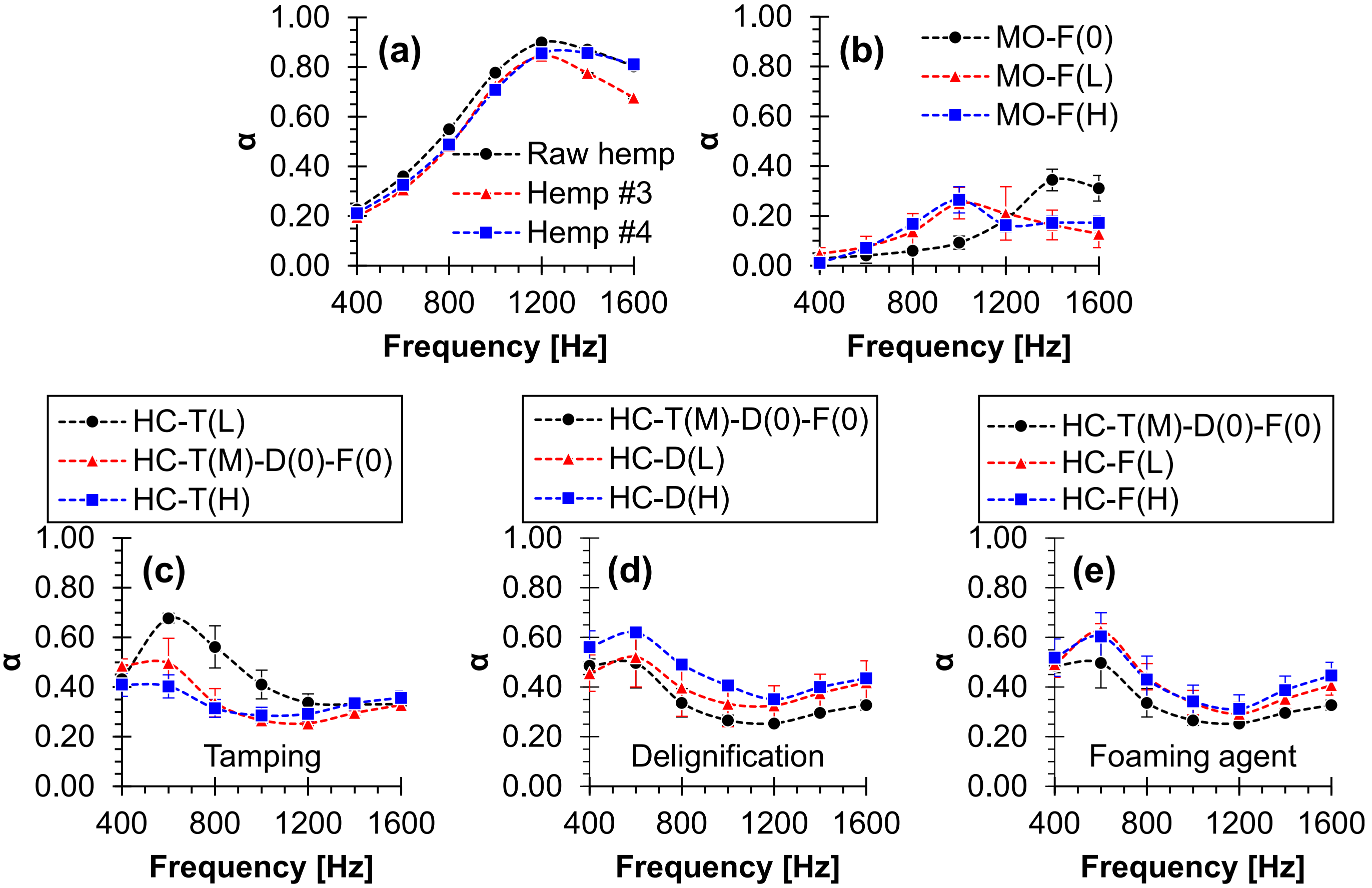

Fig. 12. The sound absorption coefficient of (a) hemp, (b) mortar, and (c-e) hempcrete samples.

reference hempcrete. In particular, HC-F(L) and HC-F(H) exhibited similar volume fractions across the three phases, indicating less effect of foaming agent addition. The detailed effects of pore modifications will be discussed in the following Section.

4. Discussion

4.1. Effects of pore modifications on hempcrete

Hempcrete contained three different porosities that exhibited varying pore shapes and sizes. For instance, the inter-pore displayed irregular-shaped pores on a mm-to-cm scale (see Fig. 15). In contrast, the hemp intra-pore featured cylinder-shaped pores sized at μm level (see Fig. 14), while the mortar intra-pore figured spherical-shaped pores [57] sized on a nm-to-μm scale (see Fig. 6). Then, this section compared three modified pores and the thermal and acoustic properties of hempcrete samples. In addition, the sound absorption at 600 Hz was selected because all hempcrete samples showed the highest α values at this frequency [see Fig. 12 (c–e)].

4.1.1. Modification of inter-pore between hemp and mortar

Fig. 17 compares the thermal conductivity, sound absorption and μCT results of hempcrete under different tamping conditions. In Fig. 17 (a), thermal conductivity increased by 67.8 %, while the sound absorption coefficient (α) decreased by 40.5 % with higher tamping conditions. In Fig. 17 (b), the total air void phase in μCT decreased by −6.4%pt. (percentage points), from 7.7 % for T(L) to 1.3 % for T(H) conditions.

First, the decreased thermal conductivity in the T(H) hempcrete shown in Fig. 17 (a) was attributed to the decrease in the cross-sectional area of the solid and the increase in the tortuosity of the heat transfer path through the pore structure [58,59]. For example, given that the air void is larger than other pores in hempcrete, it could effectively decrease the cross-sectional area of the solid. Thus, high tamping conditions reduced air void contents, negatively impacting thermal performance.

Next, as sound waves travel through and interact with the pore structure, they are converted into heat energy due to the friction of air molecules against the pore walls [60]. Meanwhile, P. Glé et al. [16] reported that high tamping conditions for hemp reduce porosity and increase density and tortuosity, but the overall acoustic performance of hempcrete is more dominated by larger pores (i.e., air void). Therefore, high tamping conditions likely reduced the air void content, which decreased the travel path of sound waves and compromised the acoustic performance.

Fig. 17 (b) also indicates that hempcrete samples exhibit inhomogeneity depending on the sample height. The upper, middle, and lower parts were quantified at 7.5, 30, and 7.5 mm heights, respectively. For example, low tamping conditions resulted in noticeable differences in the air void phase at various sample locations, while high tamping conditions minimised these differences. Moreover, for T(L) and T(M) samples, the upper part contained a significantly higher amount of air void phases. This variation was due to the compressibility and elasticity of hemp; the less compressed hemp in the upper part partially returned to its original state [10]. Consequently, in practice, achieving consistent tamping conditions throughout the height of hempcrete is challenging; thus, the thermal and soundproofing performance would change along the tamping direction of the hempcrete.

The low tamping conditions provided the best thermal and sound-absorbing performance for hempcrete, but the inhomogeneity along the height must be considered. The compressive strength of hempcrete is typically lower than 1 MPa [11,13]; thus, hempcrete is typically unsuitable for load-bearing walls due to its very low compressive strength.

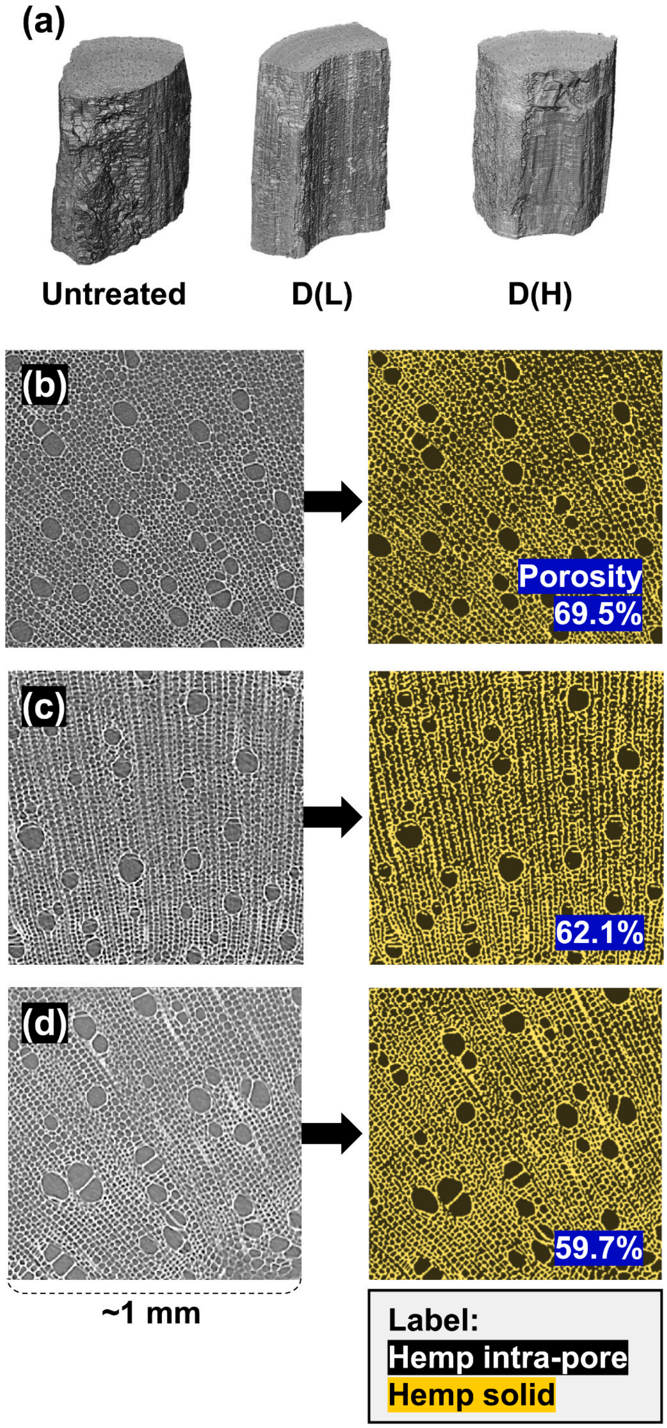

Fig. 13. Hemp segmentation results: (a) raw 3D image of hemps. Raw and segmented 2D tomograms in X-Y view under (b) untreated, (c) D(L), and (d) D (H) conditions.

The effect of tamping on compressive strength was studied by S. Benfratello et al. [13]. In their research, the hempcrete samples were prepared using similar volumes (i.e., 97–100 mm in height and 95–99 mm in diameter) but different densities (i.e., 328–955 kg/m^3) by applying different tamping conditions. They reported that hempcrete with higher density achieved higher compressive strength [13]. In this study, the degree of tamping was also proportional to the density of hempcrete (see Fig. 10); thus, the compressive strength of hempcrete was likely to increase within the same range but the compressive strength was not measured.

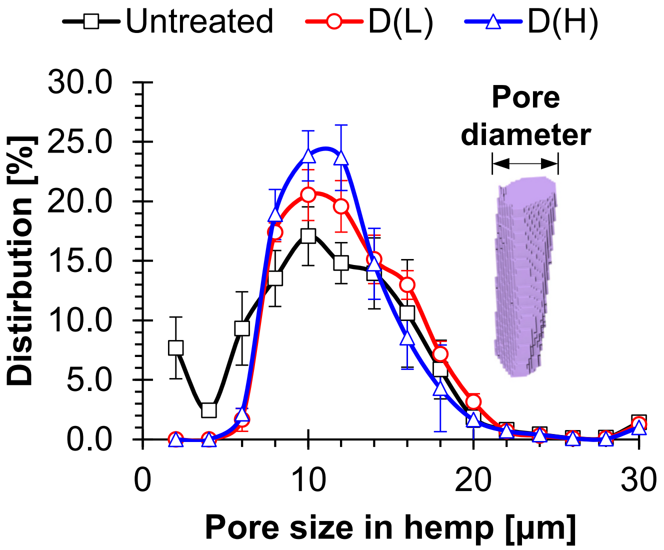

Fig. 14. Intra-pore size distribution of hemp using the suggested cylindrical pore model.

Meanwhile, tamping could affect the distribution and orientation of hemp hurds within the hempcrete samples due to the anisotropic properties of hemp hurds [61]. Moreover, S. Nguyen et al. [54] reported that transversely oriented hemp hurds contributed to better thermal insulation compared to longitudinally or randomly oriented hemp hurds based on thermal conductivity simulation. To the best of the authors' knowledge, no study has experimentally analysed the distribution and orientation of hemp hurds in hempcrete samples. In this study, the segmented hemp phase clusters were attempted to separate into single hemp hurds in the 3D tomography, but these clusters were too complicated to be separated due to insufficient μCT resolution.

4.1.2. *Modification of hemp intra-pore*

Fig. 18 compares the thermal conductivity, sound absorption, and μCT results of hempcrete under different delignification conditions. As shown in Fig. 18 (a), when the duration of the delignification process increased, the α value of hempcrete increased by 24.9 %, and both the thermal conductivities of D(H) hemp and D(H) hempcrete decreased by 23.9 % and 32.0 %, respectively compared to the D(0) hemp and D(0) hempcrete. However, in Fig. 18 (b), the total volume fractions of the hemp phase in the hempcrete samples remained more or less constant in the range between 53.2 % and 53.8 %, regardless of delignification conditions. Considering the similar volume fraction of hemp in hempcrete, the delignification process of hemp improved the thermal and acoustic properties of hempcrete. Fig. 18 (b) shows that the hemp phase varied slightly depending on the height, although the overall difference was minor.

Fig. 18 (c) shows the trend of increasing hemp pore size between 8 and 14 μm and decreasing porosity after delignification. This trend contradicts expectations, as thermal conductivity is typically lower with smaller pores for the same pore volume [62,63] or greater total porosity [64]. In this study, the treated hemp [D(L) and D(H)] exhibited higher bulk density (see Table B1). The treated hemp had thinner walls and perforated structures (see Fig. 6), and thus, these thinner walls and perforated structures might be more susceptible to shrinkage during the drying after the delignification.

It should be noted that smaller hemp hurds lead to better thermal insulation [36] and sound absorption of hempcrete [16]. Given that delignification made the hemp hurds shrink, the smaller sizes of delignified hemp hurds might have contributed to the better thermal and acoustic properties of hempcrete compared to untreated hemp hurds. Meanwhile, according to D.S. Smith et al. [64], grain size

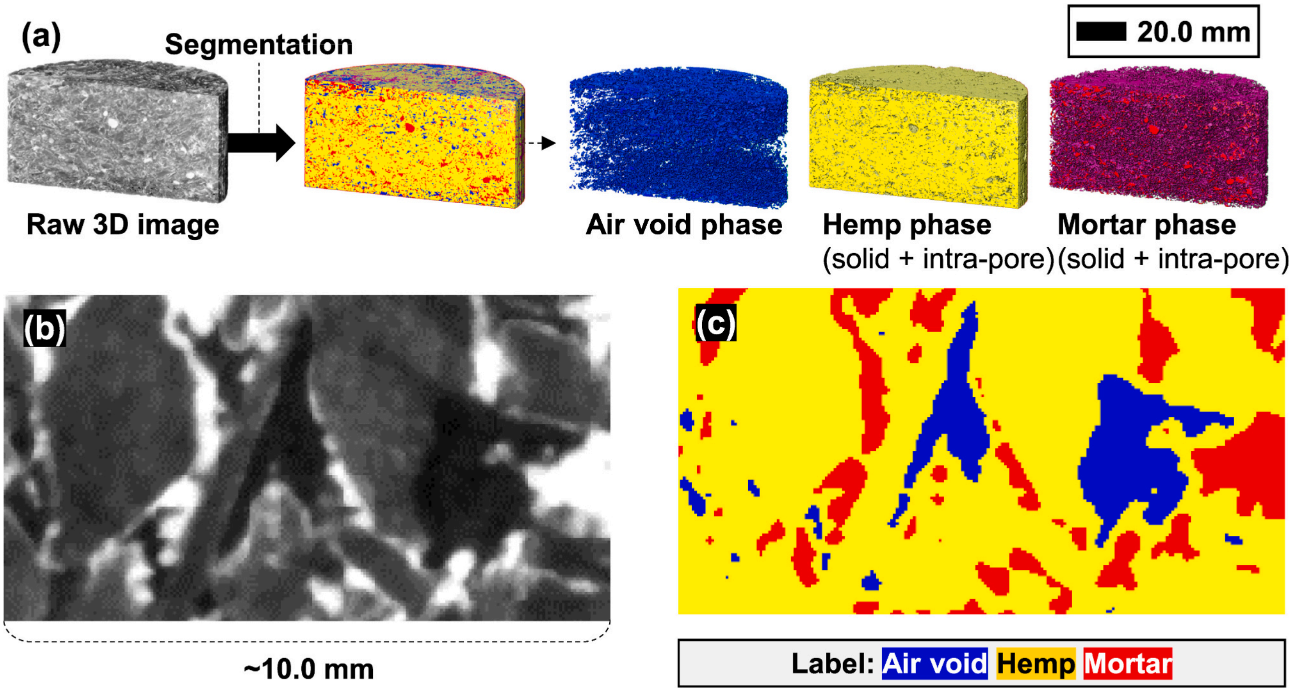

Fig. 15. Hempcrete segmentation results: (a) 3D image of hempcrete sample [e.g., HC-Ref], and sliced 2D tomograms in X-Y view (b) before and (c) after segmentation.

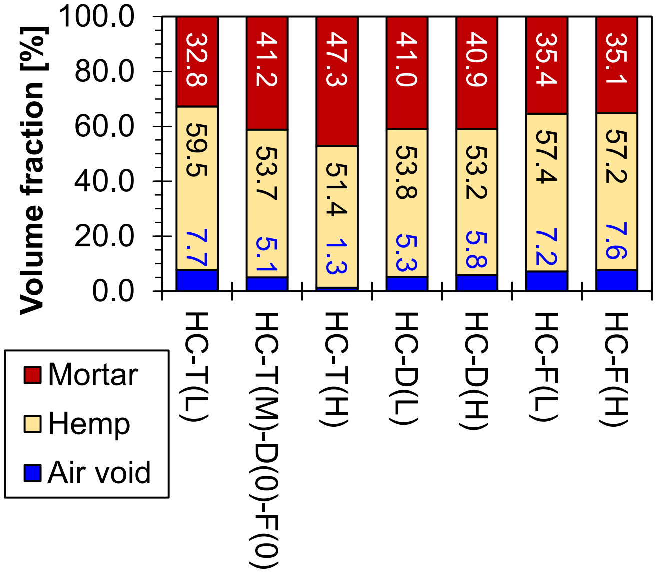

Fig. 16. Volume fractions of air void, hemp, and mortar in hempcrete samples using μCT.

significantly affected thermal conductivity more than porosity (pore volume fraction) for relatively conductive materials like ceramics. For example, smaller grain sizes can reduce the thermal conductivity of the solid phase by increasing grain boundaries along the heat path [65]. In the current study, although delignification increased the hemp pore size and decreased the hemp porosity, it eventually improved the thermal conductivity by reducing the hemp grain size. In other words, hemp grain size affected the thermal conductivity of hempcrete more than hemp intra-porosity and pore size.

Meanwhile, it should also be considered that the tamping during the fabrication of hempcrete compressed the hemp and modified the intra-pore structure of hemp. Hemp intra-porosity before the compaction seems different from its intra-porosity observed after the compaction. This effect is not taken into account in this study but will be considered in the future study.

Although the mechanical properties of hempcrete were not investigated in this study, delignification is expected to improve the mechanical properties by removing impurities on the surface of hemp hurds, improving their adhesion capacity. M.S. Tuğluca et al. [66] reported that the delignified wood fibres enhanced the adhesion of the wood fibres by removing surface impurities.

4.1.3. *Modification of mortar intra-pore*

Fig. 19 compares the thermal conductivity, sound absorption, μCT, and MIP results of hempcrete under different foaming agent conditions. The addition of foaming agents slightly reduced the thermal conductivity and showed almost negligible increase in sound absorption. However, the MIP results indicated a significant increase in mortar porosity, with a + 21.0 %pt. rise from 23.2 % for F(0) to 44.3 % for F(H) conditions.

Although pores are known to impact sound absorption and thermal insulation significantly, no remarkable performance changes were observed. This suggests that most air bubbles generated from the foaming agent were lost during sample preparation. The loss of foams is also supported by the simple calculation of the volumes of mortars for HC-Ref, HC-F(L), and HC-F(H) in Fig. 16 and Table 1. From Fig. 16, the volume ratio of mortars is 1.17:1.01:1.00 (41.2:35.4:35.1) for HC-Ref, HC-F(L), and HC-F(H). This reduced volume indicated the loss of foams during the tamping as the initial volumes of mortars (before tamping) were identical. In addition, HC-Ref, HC-F(L), and HC-F(H), respectively, have 82.7 wt%, 78.2 wt%, and 76.3 wt% of 310 g of mortar without considering foams (see Table 1.), which results in the weight ratio of 1.08:1.02:1.00 for mortars of HC-Ref, HC-F(L), and HC-F (H). GP cement particles, sand, and water can be assumed to be incompressible during the compaction. The volume ratio is similar to the weight ratio, indicating the identical density of mortars regardless of the addition of foam. Thus, the foams added to the mortar disappeared during tamping. Thus, the foams added to the mortar disappeared during tamping. This may result in a higher air void in HC-F(L) and HC-F

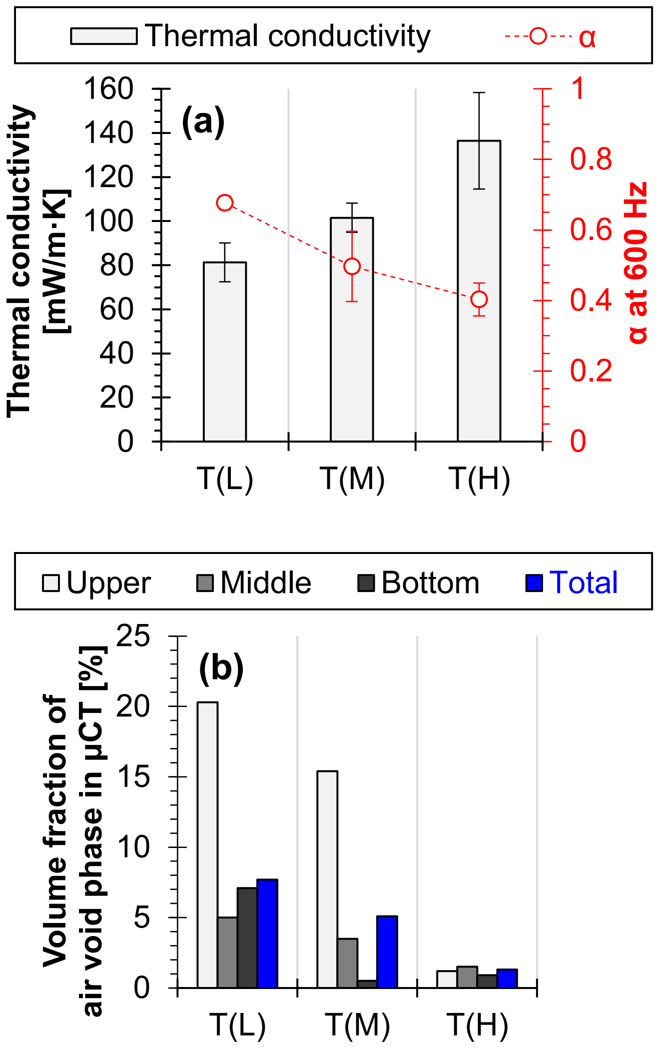

Fig. 17. Modification of inter-pore between hemp and mortar through tamping conditions: (a) thermal conductivity and sound absorption at 600 Hz and (b) volume fraction of air void phase in μCT depending on the sample height.

(H), as shown in Fig. 16. Therefore, controlling the pores in the mortar with a foaming agent was not an effective method for improving the performance of hempcrete. Given that the pores generated by the foaming agent were vulnerable to tamping conditions, future studies could safely generate micro-sized bubbles in the binder using air-entraining agents.

4.2. *Improvement of thermal and sound performances of hempcrete*

As discussed in Section 4.1, tamping conditions affected the intra-pore of mortar and hemp. Thus, only the inter-pore between hemp and mortar (i.e., air void) could be compared with the thermal and acoustic properties of hempcrete samples, as illustrated in Fig. 20. The increase in the inter-pore between hemp and mortar improved both thermal and acoustic properties of hemp. In addition, given the same mix design and the same degree of compaction, the use of delignified hemp improved the thermal and acoustic properties of hempcrete.

Consequently, increasing the inter-porosity between hemp and mortar was the optimal method for developing thermal insulating and soundproof material, achievable through low tamping and high delignification conditions. On the other hand, foaming agent conditions were ineffective in improving both performances.

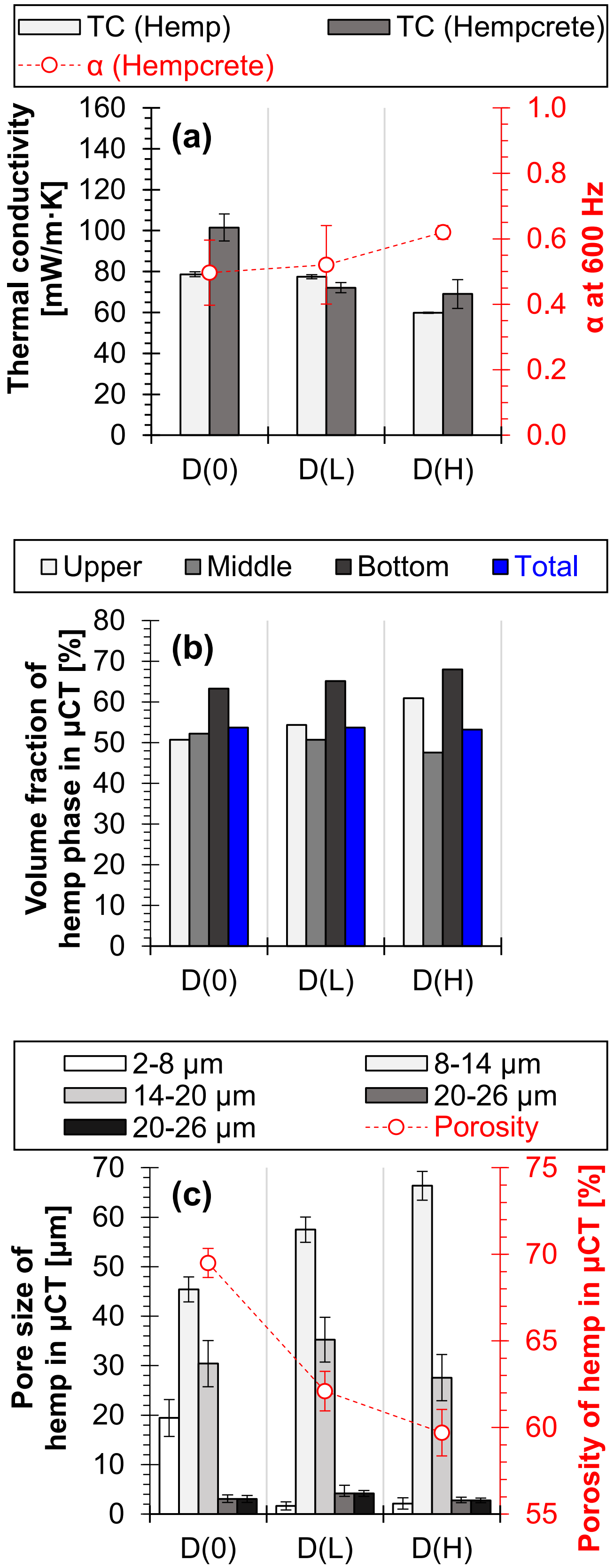

Fig. 18. Modification of hemp intra-pore through delignification conditions: (a) thermal conductivity and sound absorption at 600 Hz, (b) volume fraction of hemp phase in μCT depending on the sample height, and (c) pore size and porosity of hemp in μCT.

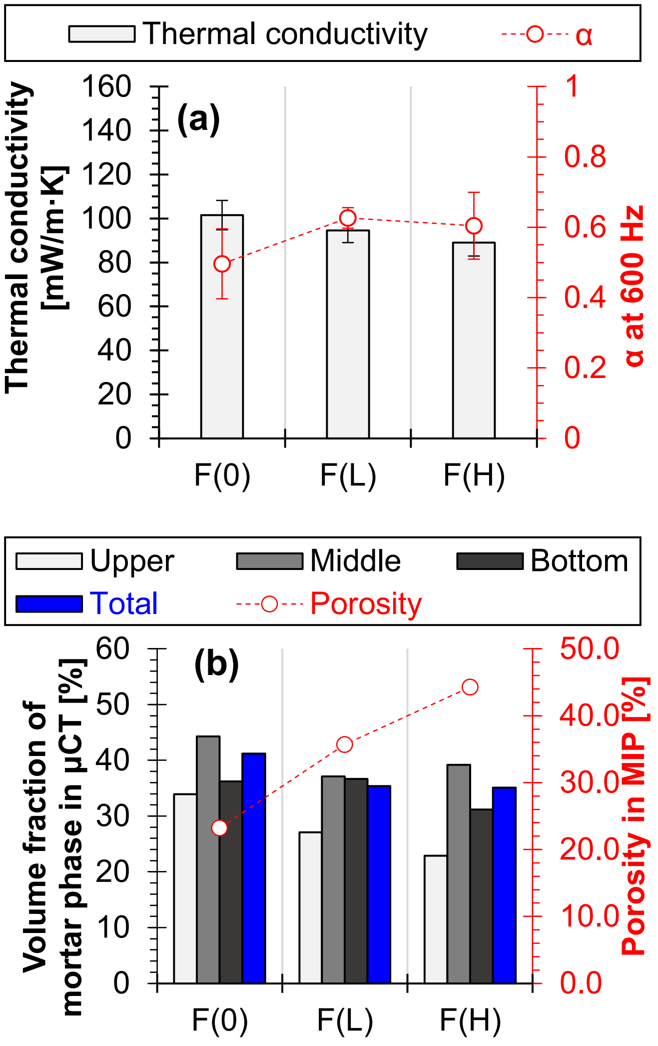

Fig. 19. Modification of mortar intra-pore through foaming agent conditions: (a) thermal conductivity, sound absorption at 600 Hz and (b) volume fraction of mortar phase in μCT depending on the sample height and porosity in MIP.

5. Conclusions

As thermal insulating and soundproofing cementitious materials have been widely developed by utilising lightweight porous composites, hempcrete has been widely used as a lightweight material. Therefore, pore analysis on lightweight materials, including hempcrete, is crucial to these performance-based material designs. The present study investigates the effects of the three different pores in hempcrete (i.e., inter-pore between hemp and mortar, hemp intra-porosity, and mortar intra-pore) on hempcrete acoustic and thermal properties. The three different porosities were modified by tamping, delignification, and foaming agent usage. It should be highlighted that the present study newly developed thorough techniques to segment the hempcrete phases in μCT images to understand its intra-porosity and intra-pore size distribution. The significant findings are as follows:

- In μCT analysis, hemp intra-porosity (59.7–69.5 %) was assessed by thresholding method using the Otsu mode. Moreover, a novel cylindrical pore model was suggested to estimate the distribution of its intra-pore sizes (2–30 μm). Then, hempcrete samples were segmented using thresholding methods with subvolume extraction, colour map histograms, and deconvolution techniques.
- Hempcrete samples exhibited significant inhomogeneity along its height; thus, the thermal and acoustic properties seem to be the function of the height of the hempcrete. Moreover, they exhibited time-dependent behaviour, with 10.7–17.4 % bulk density changes over a 28-day curing period and were identified as multiple phases.
- The inter-pore between hemp and mortar exhibited a significant correlation with thermal and acoustic properties compared to hemp or mortar intra-pores. Higher tamping conditions significantly decreased the inter-porosity between hemp and mortar. In other words, low tamping was the optimum approach for developing thermal insulation and sound-absorbing materials despite the consideration of potential reductions in the mechanical strength of hempcrete and inhomogeneity depending on sample height.
- High delignification conditions also improved the thermal performance of hempcrete by increasing the grain number of hemp. Although the intra-pore structure in hemp was significantly reduced due to its compressibility, delignification effectively improved the thermal and acoustic performances of hempcrete samples.
- The foaming agent was used to modify the intra-pore structure of the cement mortar, leading to a reduction in total porosity from 23.2 % to 44.3 % and bulk density from 22.8 % to 29.1 % as measured by MIP analysis. However, the thermal and acoustic performances were

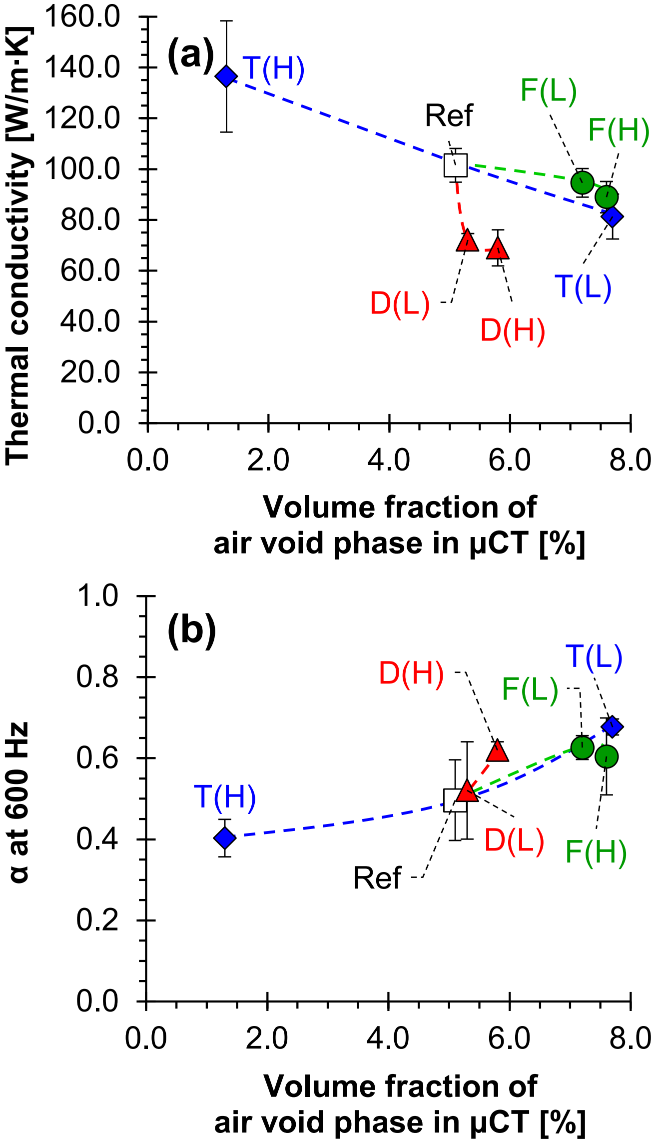

Fig. 20. Correlation of the volume fraction of air void phases in μCT with (a) thermal conductivity and (b) sound absorption coefficient at 600 Hz.

not significantly improved, likely due to the loss of most air bubbles during sample preparation.

- Future study will investigate the effect of compressive forces on the hemp intra-pore to understand the actual porosity of hemp in hempcrete. Moreover, the entrained air will be applied into the cementitious mortar in hempcrete to generate micro-bubbles inside the binder because the current mortar intra-pore generated by the foaming agent was vulnerable to compressive forces.

Many hempcrete samples have been developed as thermal insulating or soundproofing materials because they are used as sound-absorbing or thermally insulating building elements (e.g., wall and roof) in real-world hempcrete applications. These performances highly depend on pore structure, but pore analysis for hemp and hempcrete has been challenging due to their inhomogeneity, multiphase composition, and time dependency. The current study suggests a new μCT segmentation method for hemp and hempcrete to understand the pore structure, including size, shape, and quantity. This method successfully segmented the inter pores (air voids), hemp, and binder phases and can be readily expanded to analyse any porous structure of the multiphase materials. The 3D data of the porous system inside hempcrete can be used to investigate the properties of porous structures and to combine with the computational modelling for porous systems. However, there is still a challenge in segmenting the interface between hemp and mortar. In addition, to analyse the intra-pores of hemp and mortar phases, small-sized samples should be separately prepared to obtain μCT images with sufficiently high resolution.

Author statement

All persons who meet authorship criteria are listed as authors, and all authors certify that they have participated sufficiently in the work to take public responsibility for the content, including participation in the concept, design, analysis, writing, or revision of the manuscript.

CRediT authorship contribution statement

Haemin Song: Writing – original draft, Visualization, Validation, Methodology, Investigation, Formal analysis, Data curation, Conceptualization. **Taehwan Kim:** Writing – review & editing, Validation, Supervision, Resources, Methodology, Investigation, Formal analysis, Conceptualization. **Ailar Hajimohammadi:** Writing – review & editing, Validation, Supervision. **Jae Eun Oh:** Writing – review & editing, Validation, Supervision. **Arnaud Castel:** Writing – review & editing, Validation, Methodology, Funding acquisition, Formal analysis.

Declaration of competing interest

The authors declare that they have no known competing financial interests or personal relationships that could have appeared to influence the work reported in this paper.

Acknowledgement

This work was supported by a research grant from Australian Research Council and Australian Hemp Mansory Pty Ltd. (ARC Linkage project, LP200200779 titled "Decarbonising built environments with hempcrete and green wall technology"). The content of this paper reflects the views of the authors, who are responsible for the facts and the accuracy of the data presented herein and does not necessarily reflect the official view of Australian Hemp Manosry Pty Ltd. nor does the contents constitute a standard, specification or regulation. This work was also supported by the government of the Republic of Korea (MSIT) and the National Research Foundation of Korea (NRF-2023K2A9A1A01098453) for collaborative work between UNSW and UNIST.

Appendix A. Hemp sieving

Table A1 shows the residual weight percentage of raw hemp after sieving. Initially, 150.0 g of hemp was sieved for 30 min to achieve a thorough separation. The hemp exhibited considerable variation in size and shape (see Fig. 2), with the majority classified as hemp #3 and #4. The ratio between hemp #3 and #4 was approximately 1.62. Therefore, the present study used hemp #3 and #4 to prevent hemp size and shape inhomogeneity.

However, sieving for 30 min each time was inefficient in providing sufficient hemp needed for this study. As a result, hemp #3 and #4 were obtained by sieving 150.0 g of hemp 13 times for 10 min each. Although the quantity of hemp classified through 10-minute sieving differed from that of 30-minute sieving, the size of the hemp used in this study was consistent.

Table A1
The weight percentage of raw hemp sieved once for 30 min and 13 times for 10 min.

Label	Size [mm]	Residual weight percentage [%]	
		1 time for 30 mins	13 times for 10 mins
Hemp #1	4.75–9.5	2.61	4.50
Hemp #2	4.75–9.5	2.68	18.82
Hemp #3	2.36–4.75	35.43	24.26
Hemp #4	1.18–2.36	40.72	39.49
Hemp #5	0.6–1.18	7.97	9.62
Hemp #6	0.3–0.6	5.43	1.61
Hemp #7	0.15–0.3	2.01	0.96
Hemp #8	< 0.15	3.15	0.74
Sum		100.00	100.00

Appendix B. Bulk density of hemp and mortar

Table B1 shows the bulk density of the materials used in this study. Triplicate samples were measured to calculate the average values and standard deviations.

Table B1
Bulk density of sand, fresh mortar, and hemp. D(L) and D(H) denote delignified conditions for 1 and 3 h, respectively. Oven drying condition denotes 80 °C for 72 h in the oven.

Label	Conditions		Bulk density (kg/m^3)	Label	Conditions		Bulk density (kg/m^3)
Sand	–	Air	1512.4 (± 2.3)	Hemp #5	–	Air	104.9 (± 2.9)
MO-Ref	–	–	1563.2 (± 40.9)	Hemp #6	–	Air	92.1 (± 6.8)
MO-F(0)	–	–	1955.2 (± 47.2)	Hemp #7	–	Air	55.8 (± 5.4)
MO-F(L)	–	–	1509.7 (± 39.2)	Hemp #8	–	Air	39.3 (± 0.5)
MO-F(H)	–	–	1386.6 (± 15.4)	Hemp #3	–	Oven	92.4 (± 3.4)
Raw hemp	–	Air	107.2 (± 2.6)	Hemp #3	D(L)	Oven	102.1 (± 3.3)
Hemp #1	–	Air	99.4 (± 2.6)	Hemp #3	D(H)	Oven	117.0 (± 2.3)
Hemp #2	–	Air	54.5 (± 8.9)	Hemp #4	–	Oven	87.9 (± 0.7)
Hemp #3	–	Air	107.1 (± 0.8)	Hemp #4	D(L)	Oven	91.2 (± 1.4)
Hemp #4	–	Air	101.8 (± 3.2)	Hemp #4	D(H)	Oven	96.4 (± 1.3)

Appendix C. Tomogram segmentations of hemp

Fig. C1 shows the entire process of segmenting intra-porosity in hemp under untreated, D(L), and D(H) conditions using Avizo and ImageJ software. First, as illustrated in Fig. C1 (a), 2600 raw 2D scan images were collected and filtered using a median filter to reduce noise. Then, a mask image was created corresponding to the hemp volume to remove areas outside the mask. Next, 5 cubic subvolumes (~0.5 mm) were extracted from the hemp at constant intervals. A total of 15 sliced images were saved from the three different slices (upper, middle, and bottom) of the 5 subvolumes.

Next, since ImageJ software offered 17 different thresholding modes, all modes were applied to the 15 images obtained 5 cubic subvolumes. It should be noted that the appropriate thresholding mode selection was significant for segmenting the intra-pore of hemp. For example, Fig. C1 (b) shows the segmented images of hemp using three of the 17 thresholding modes (i.e., Percentile, Otsu, and Max entropy modes). The Percentile mode overestimated the solid phase by identifying solid phases inside the hemp pore, while the Max entropy mode underestimated the solid phase as the plant wall structure was not identified. On the contrary, the Otsu mode accurately identified the solid and intra-pore phases of hemp without mis-estimations. Therefore, the present study applied the Otsu mode to the 15 images; thus, 15 thresholding values were obtained. Finally, the final thresholding value was selected by averaging these 15 thresholding values and used to segment the 3D hemp segmentation.

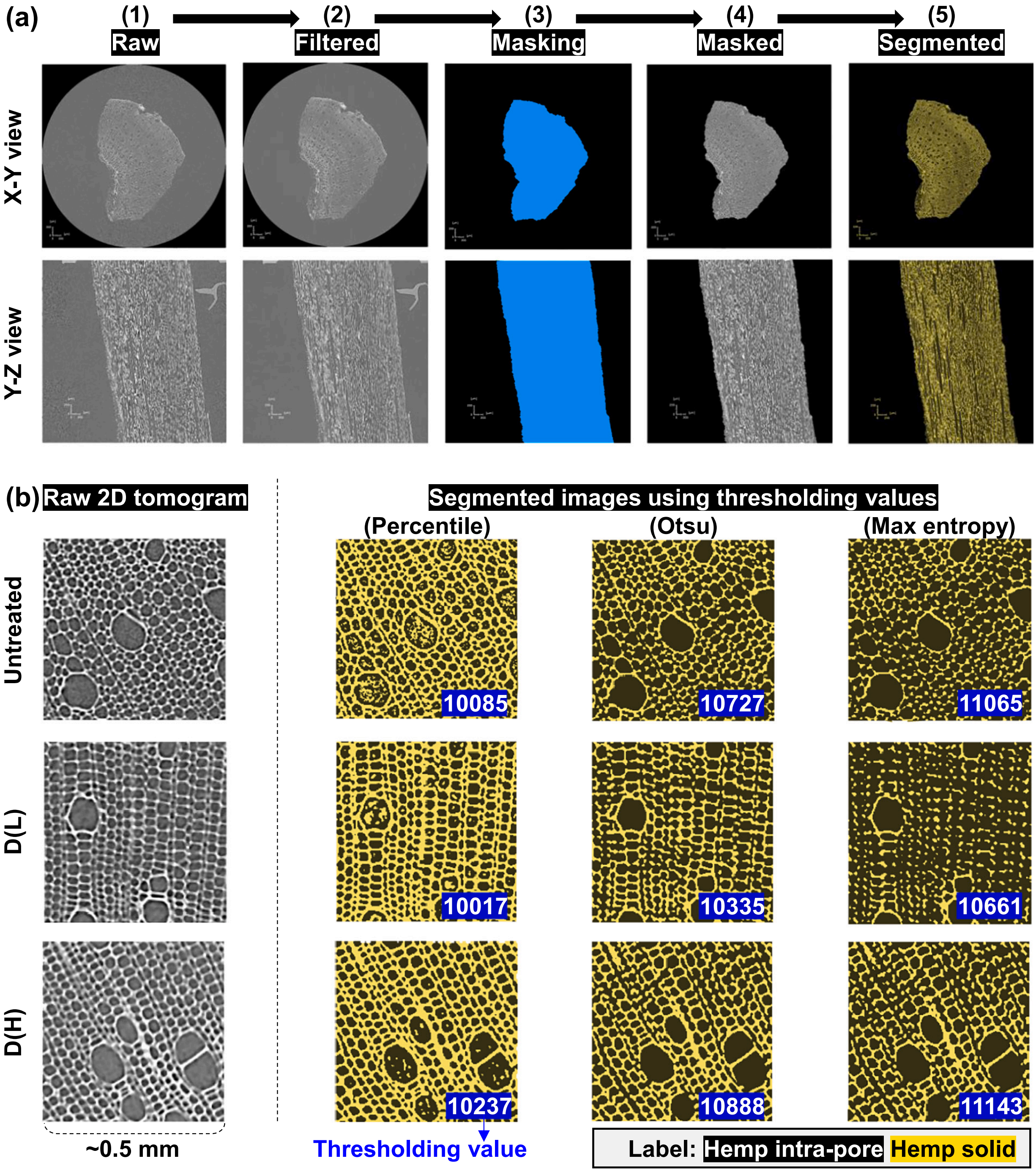

Fig. C1. Hemp intra-porosity segmentation using Aviso and ImageJ software: (a) segmenting process in X-Y and Y-Z view and (b) segmented images with different thresholding modes (Percentile, Otsu, and Max entropy).

Appendix D. Cylindrical pore model of hemp

The present study proposed a cylindrical pore model of hemp to calculate the hemp intra-pore diameter. The cylinder-shaped pores of hemp were observed from the hemp segmentation, as shown in Fig. D1. Unfortunately, Avizo software did not directly provide the diameter of the cylindrical elements. However, this software offered informative properties such as the volume and surface area computed from voxel counting. Thus, in this study, the segmented intra-pores in hemp from 5 subvolumes (see Appendix C) were split into individual cylindrical pores using the label analysis function in Avizo software. Afterward, the pore volume and the surface area of each cylindrical pore could be computed. Finally, from the equations of the volume and surface area of the cylinder (see Eqs. (D1) and (D2), respectively), the cylindrical pore radius (or even diameter) could be computed by MATLAB software using Eq. (D3), where r and h were the radius and height of the cylinder, respectively.

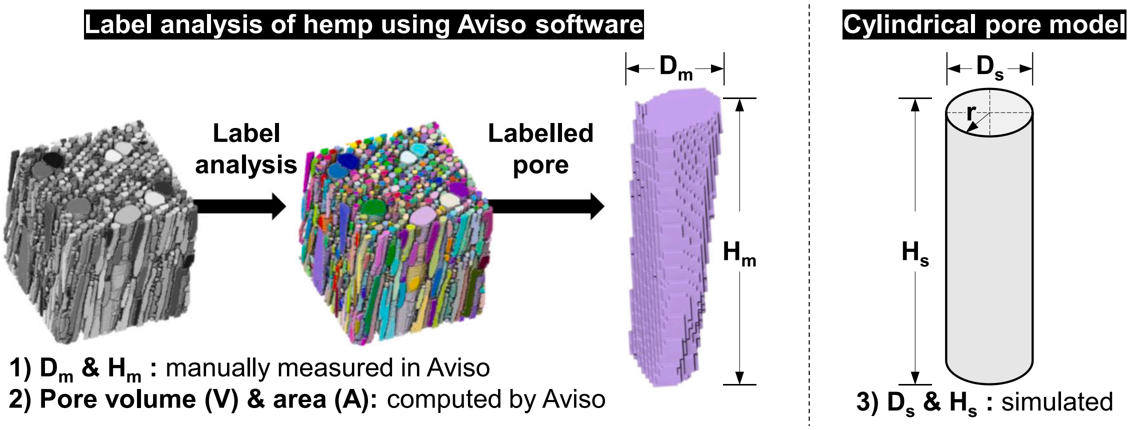

Fig. D1. The schematic diagram of the suggested cylindrical pore model of hemp.

$$\mathrm{V} = \pi \mathrm{r}^2 \times h \tag{D1}$$

$$\mathrm{A} = 2\pi \mathrm{r}^2 + 2\pi \mathrm{r} \times h \tag{D2}$$

$$2\pi \mathrm{r}^3 - \mathrm{Ar} + 2\mathrm{V} = 0 \tag{D3}$$

The simulated pore diameter ($D_s = 2r$) was computed using the cylindrical pore model, while the diameter (D_m) and height (H_m) were manually measured using the measure tool in Avizo software. In particular, because the pore shape of hemp was not perfectly cylindrical, the longest diameter was used as D_m value. Meanwhile, given that one of the subvolumes of hemp #3 contained 859 intra-pores, D_m of 100 out of the total pores was compared with D_s to verify the suggested model. As illustrated in Fig. D2, the simulated diameter showed a high correlation ($R^2 = 0.91$) with the measured diameter, supporting using the cylindrical pore model to calculate the entire intra-pore sizes of hemp.

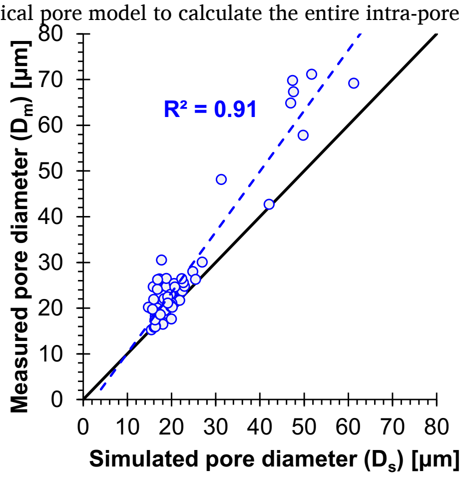

Fig. D2. Comparison of D_m and D_s to verify the cylindrical pore model.

Appendix E. Tomogram segmentations of hempcrete

Since the entire hempcrete sample included three phases (air void, hemp, and mortar), two thresholding values were necessary to delineate the boundaries between air void-to-hemp and hemp-to-mortar. However, as shown in the colour map histogram of the HC-Ref sample [see Fig. E1 (a)], this histogram could not provide meaningful thresholding values because all phases overlapped.

Furthermore, when arbitrary thresholding values were applied to the entire hempcrete sample, the 3D tomogram underestimates the air void phase depending on the sample height [see red box in Fig. E1 (b)]. These air void differences appeared vertical rather than lateral; thus, the tamping condition influenced this difference more than the drying effect. Moreover, the part of the hemp phase could be misidentified as the air void phase [see red box in Fig. E1 (d)]. Thus, hempcrete segmentation required considerable thresholding value selections even if it was challenging due to the following factors: i) their multiphase compositions, ii) inhomogeneity due to the compressibility of hemp unlike other phases, and iii) the time-dependency related to curing and storage conditions.

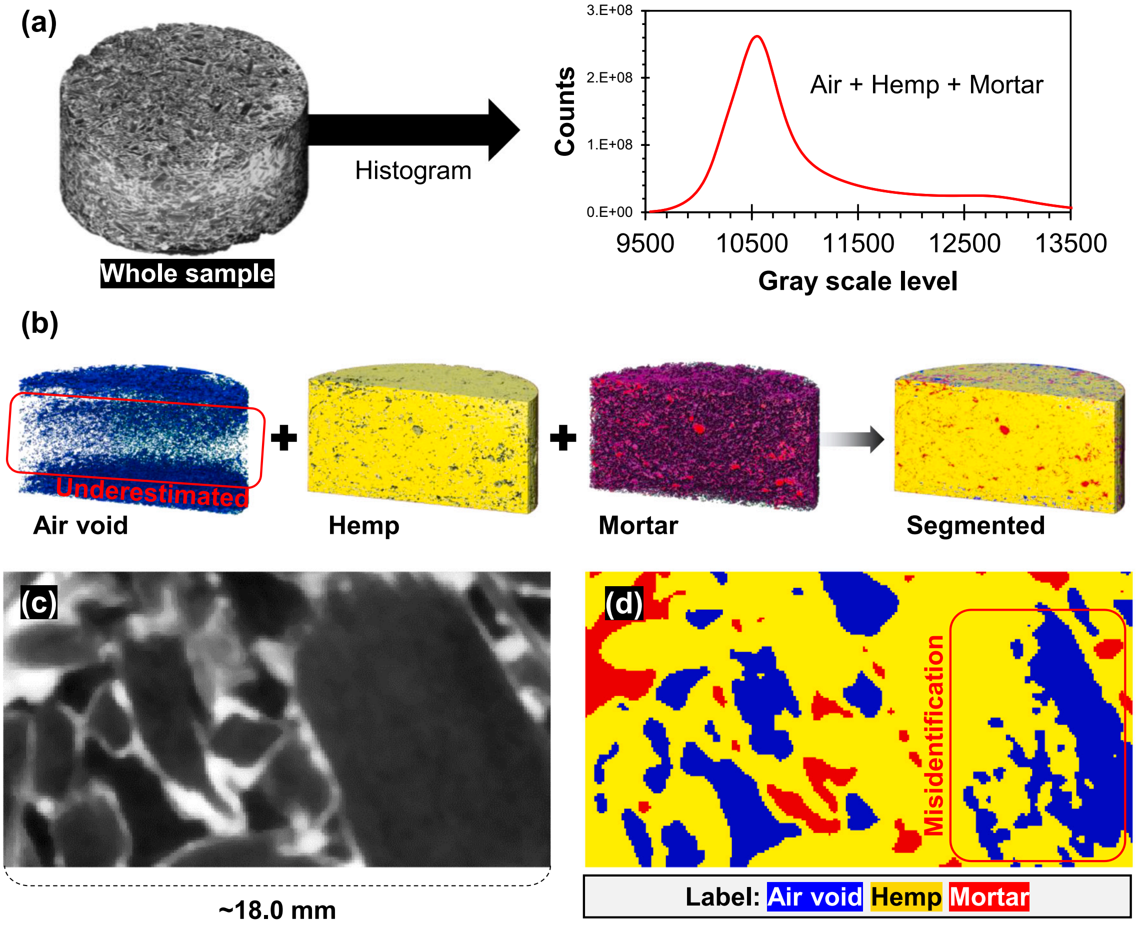

Fig. E1. Examples of difficulty in hempcrete segmentation: (a) colour map histogram of the entire hempcrete sample, (b) 3D image of hempcrete sample (HC-Ref) after improper segmentation. 2D sliced tomograms (b) before and (c) after improper segmentation.

Despite the limitations of μCT on hempcrete segmentations, the present study proposed the deconvolution method to reasonably compute two thresholding values from the hempcrete samples (see Fig. E2). In particular, Fig. 4 showed the whole hempcrete segmentation process using Aviso software, and cubic subvolumes (~6.5 mm) were extracted from each part (the upper, middle, and bottom). Unlike the colour map histogram of the entire sample [see Fig. E1 (a)], that of the extracted subvolumes [see Fig. E2 (a)] had a distinct peak, indicating the air void phase of the hempcrete sample. Based on the peak, deconvoluted peaks were generated using the Gaussian distribution model with the optimal mean and standard deviation. The optimal values were selected when the error between the measured histogram and the calculated one was smallest.

Fig. E2 (b) shows the enlarged deconvoluted peaks of the subvolume from the middle part. The first thresholding value between air void-to-hemp was selected as the intersection of those deconvoluted peaks. However, the deconvolution method unexpectedly identified the interphase of hemp-mortar [see Fig. E2 (c)]. Since it was almost impossible to divide this phase precisely, the second thresholding value between hemp and mortar was selected as the average value of the intersection of hemp and interphase peaks and that of interphase and mortar peaks. Finally, two thresholding values were applied to each part to segment air void, hemp, and mortar. Afterwards, the volume fractions of each phase for the entire hempcrete sample were calculated by merging the fractions from each part.

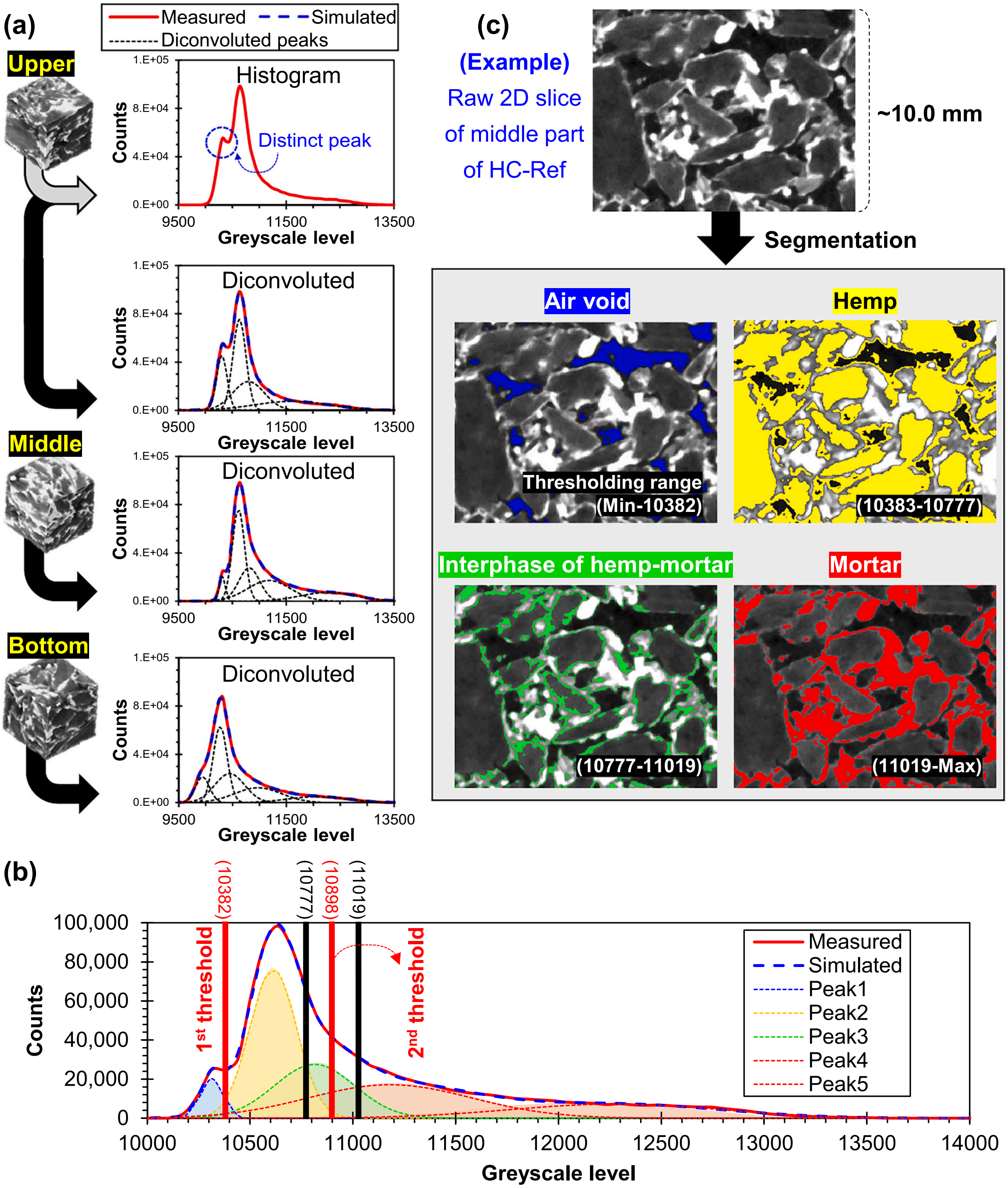

Fig. E2. Hempcrete segmentation using Aviso software: (a) colour map histogram of the subvolumes using deconvolution method, (b) enlarged histogram of subvolume from the middle part, and (c) segmented images of HC-Ref.

To validate the hempcrete segmentation, the volume fraction of mortar was roughly estimated according to Eqs. (E1)–(E2). First, only hemp was assumed to be compressible, while other materials (cement, sand, and water) were incompressible. Next, the density of GP cement (ρ_c), sand (ρ_s), and water (ρ_w) were assumed as 3.1 [67], 2.65 [68], and 1.0 g/cm^3, respectively. Then, the volume fraction of mortar for HC-T(L), HC-T(M), and HC-T(H) were calculated as 35.8, 41.1, and 45.1 %, respectively. Therefore, hempcrete segmentations in μCT showed well-matched validation because these values were almost similar to their volume fractions of mortar (32.8, 41.2, and 47.3 %, respectively, as shown in Fig. 16).

$$\rho_M = (m_c + m_s + m_w) \Big/ \left(\frac{m_c}{\rho_c} + \frac{m_s}{\rho_s} + \frac{m_w}{\rho_w} \right) \tag{E1}$$

$$\varphi_M = \frac{W_H}{\rho_M \bullet V_{Mld}} \times \left(\frac{m_c + m_s + m_w}{m_c + m_s + m_w + m_h} \right) \times 100 \tag{E4}$$

where $m_{c,\ s,\ w,\ \text{and}\ h}$ was the mass of materials (cement, sand, water, and hemp, respectively); $\rho_{M,\ c,\ s,\ w}$ was the density of materials (cement mortar, cement, sand, and water, respectively); φ_M was the volume fraction of cement mortar; W_H was the added weight of fresh hempcrete (e.g., 270, 310, and 340 g for hempcrete under T(L), T(M), and T(H) conditions, respectively); and V_{Mld} was the volume of used 3D printed mould (384.69 cm^3).

Finally, Fig. E3 shows the segmented hempcrete samples. High tamping conditions noticeably increased mortar phases while air void and hemp phases decreased. Volume fractions of all phases were compared in Fig. 16.

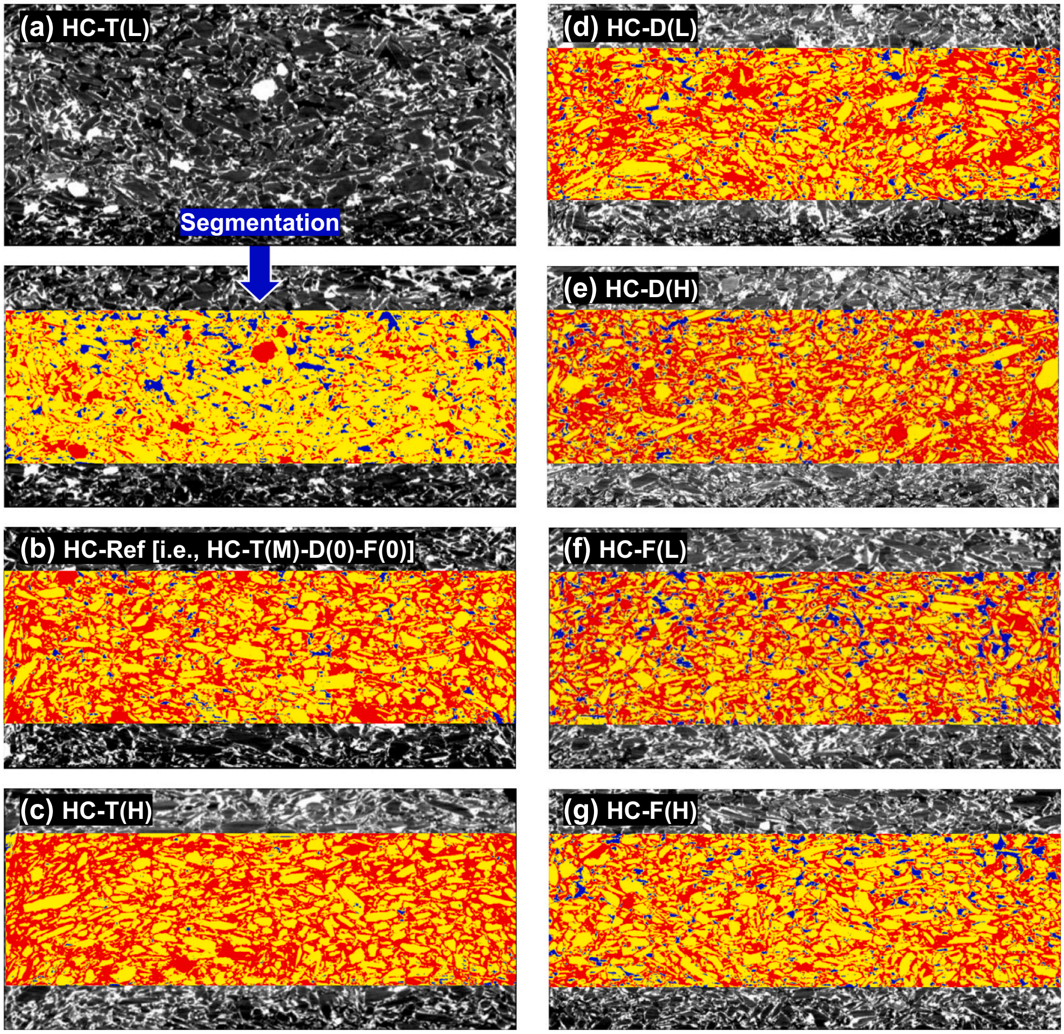

Fig. E3. Segmented middle parts of all hempcrete samples: (a) filtered and segmented image of HC-T(L), and (b-g) segmented images of other hempcrete samples. Blue, yellow, and red labels denote air void, hemp, and mortar phases, respectively. (For interpretation of the references to colour in this figure legend, the reader is referred to the web version of this article.)

Data availability

Data will be made available on request.

References

[1] A. Arrigoni, R. Pelosato, P. Melià, G. Ruggieri, S. Sabbadini, G. Dotelli, Life cycle assessment of natural building materials: the role of carbonation, mixture components and transport in the environ- mental impacts of hempcrete blocks, J. Clean. Prod. 149 (2017) 1051–1061.

[2] T. Jami, S. Karade, L. Singh, A review of the properties of hemp concrete for green building applications, J. Clean. Prod. 239 (2019) 117852.

[3] A. Piot, T. Béjat, A. Jay, L. Bessette, E. Wurtz, L. Barnes-Davin, Study of a hempcrete wall exposed to outdoor climate: effects of the coating, Construct. Build Mater. 139 (2017) 540–550.

[4] M. Degrave-Lemeurs, P. Gle, A.H. de Menibus, Acoustical properties of hemp concretes for buildings thermal insulation: application to clay and lime binders, Construct. Build Mater. 160 (2018) 462–474.

[5] G. Balčiūnas, J. Žvironaitė, S. Vėjelis, A. Jagniatinskis, S. Gaidučis, Ecological, thermal and acous- tical insulating composite from hemp shives and sapropel binder, Ind. Crop. Prod. 91 (2016) 286–294.

[6] S. Hetimy, N. Megahed, O.A. Eleinen, D. Elgheznawy, Exploring the potential of sheep wool as an eco-friendly insulation material: a comprehensive review and analytical ranking, sustainable, Sustain. Mater. Technol. 39 (2023) e00812, https://doi.org/10.1016/j.susmat.2023.e00812.

[7] J.-X. Lu, P. Shen, H. Zheng, H.A. Ali, C.S. Poon, Development and characteristics of ultra high-performance lightweight cementitious composites (UHP-LCCs), Cem. Concr. Res. 145 (2021) 106462.

[8] A. Bouguerra, A. Ledhem, F. De Barquin, R. Dheilly, M. Quéneudec, Effect of microstructure on the mechanical and thermal properties of lightweight concrete prepared from clay, cement, and wood aggregates, Cem. Concr. Res. 28 (1998) 1179–1190.

[9] H.-K. Kim, J. Jeon, H.-K. Lee, Workability, and mechanical, acoustic and thermal properties of lightweight aggregate concrete with a high volume of entrained air, Construct. Build Mater. 29 (2012) 193–200.

[10] P. Glé, E. Gourdon, L. Arnaud, Acoustical properties of materials made of vegetable particles with several scales of porosity, Appl. Acoust. 72 (2011) 249–259.

[11] S. Elfordy, F. Lucas, F. Tancret, Y. Scudeller, L. Goudet, Mechanical and thermal properties of lime and hemp concrete (“hempcrete”) manufactured by a projection process, Construct. Build Mater. 22 (2008) 2116–2123.

[12] U. Dhakal, U. Berardi, M. Gorgolewski, R. Richman, Hygrothermal performance of hempcrete for Ontario (Canada) buildings, J. Clean. Prod. 142 (2017) 3655–3664.

[13] S. Benfratello, C. Capitano, G. Peri, G. Rizzo, G. Scaccianoce, G. Sorrentino, Thermal and structural properties of a hemp–lime biocomposite, Construct. Build Mater. 48 (2013) 745–754.

[14] Y.W. Shewalul, N.F. Quiroz, D. Streicher, R. Walls, Fire behavior of hemp blocks: a biomass-based construction material, J. Build. Eng. 80 (2023) 108147.

[15] R. Walker, S. Pavia, R. Mitchell, Mechanical properties and durability of hemp-lime concretes, Construct. Build Mater. 61 (2014) 340–348.

[16] P. Glé, E. Gourdon, L. Arnaud, Modelling of the acoustical properties of hemp particles, Construct. Build Mater. 37 (2012) 801–811.

[17] A. Hajimohammadi, T. Ngo, P. Mendis, A. Kashani, J.S. van Deventer, Alkali activated slag foams: the effect of the alkali reaction on foam characteristics, J. Clean. Prod. 147 (2017) 330–339.

[18] A. Siddika, T. Kim, V. Sahajwalla, A. Hajimohammadi, Early age structural build-up and pore stability in raw foam at ambient conditions: implications for the final properties of glass-ceramic foam, Construct. Build Mater. 428 (2024) 136369.

[19] A.P. Manian, M. Cordin, T. Pham, Extraction of cellulose fibers from flax and hemp: a review, Cellulose 28 (2021) 8275–8294.

[20] N. Mokshina, T. Chernova, D. Galinousky, O. Gorshkov, T. Gorshkova, Key stages of fiber development as determinants of bast fiber yield and quality, Fibers 6 (2018) 20.

[21] X. Zhao, Y. Liu, L. Zhao, A. Yazdkhasti, Y. Mao, A.P. Siciliano, J. Dai, S. Jing, H. Xie, Z. Li, A scalable high-porosity wood for sound absorption and thermal insulation, Nat. Sustain. 6 (2023) 306–315.

[22] A. Bledzki, J. Gassan, Composites reinforced with cellulose based fibres, Prog. Polym. Sci. 24 (1999) 221–274.

[23] A. Mohanty, M. Misra, L.T. Drzal, Surface modifications of natural fibers and performance of the resulting biocomposites: an overview, Compos. Interfaces 8 (2001) 313–343.

[24] M. Kabir, H. Wang, K. Lau, F. Cardona, T. Aravinthan, Mechanical properties of chemically-treated hemp fibre reinforced sandwich composites, Compos. Part B Eng. 43 (2012) 159–169.

[25] I. Ceyte, Béton de chanvre, définition des caractéristiques mécaniques de la chènevotte, Travail de fin d’études, ENTPE 155 (2008) 2008.

[26] P. Łapka, F. Dietrich, P. Furmański, M. Sinka, G. Sahmenko, D. Bajare, Experimental and numerical estimation of thermal conductivity of bio-based building composite materials with an enhanced thermal capacity, J. Energy Storage 97 (2024) 112943.

[27] S. Tulip, N. Sarker, N. Nahar, M. Yang, E. Monono, Effect of process parameters on the physical and mechanical properties of cornstarch-based construction materials, Constr. Mater. 3 (2023) 320–336.

[28] M. Wevers, B. Nicolaï, P. Verboven, R. Swennen, S. Roels, E. Verstrynge, S. Lomov, G. Kerckhofs, B. Van Meerbeek, A.M. Mavridou, Applications of CT for non-destructive testing and materials charac- terization, Ind. X-ray Comput. Tomogr. (2018) 267–331.

[29] T. Kim, M.F. Alnahhal, Q.D. Nguyen, P. Panchmatia, A. Hajimohammadi, A. Castel, Initial sequence for alkali-silica reaction: transport barrier and spatial distribution of reaction products, Cem. Concr. Compos. 104 (2019) 103378.

[30] M. Shakoorioskooie, M. Griffa, A. Leemann, R. Zboray, P. Lura, Alkali-silica reaction products and cracks: X-ray micro-tomography-based analysis of their spatial-temporal evolution at a mesoscale, Cem. Concr. Res. 150 (2021) 106593.

[31] Q. Hu, M. Aboustait, T. Kim, M.T. Ley, J.C. Hanan, J. Bullard, R. Winarski, V. Rose, Direct three-dimensional observation of the microstructure and chemistry of C3S hydration, Cem. Concr. Res. 88 (2016) 157–169.

[32] Q. Hu, M. Aboustait, T. Kim, M.T. Ley, J.W. Bullard, G. Scherer, J.C. Hanan, V. Rose, R. Winarski, J. Gelb, Direct measurements of 3d structure, chemistry and mass density during the induction period of C3s hydration, Cem. Concr. Res. 89 (2016) 14–26.

[33] Z. Wu, Y. Wei, S. Wang, J. Chen, Application of X-ray micro-CT for quantifying degree of hydration of slag-blended cement paste, J. Mater. Civ. Eng. 32 (2020) 04020008.

[34] J.-S. Kim, J.H. Kim, T.-S. Han, Microstructure characterization of cement paste from micro-CT and correlations with mechanical properties evaluated from virtual and real experiments, Mater. Charact. 155 (2019) 109807.

[35] J. Schock, S. Liebl, K. Achterhold, F. Pfeiffer, Obtaining the spacing factor of microporous concrete using high-resolution dual energy X-ray Micro CT, Cem. Concr. Res. 89 (2016) 200–205.

[36] E. Gourlay, P. Glé, S. Marceau, C. Foy, S. Moscardelli, Effect of water content on the acoustical and thermal properties of hemp concretes, Construct. Build Mater. 139 (2017) 513–523.

[37] B. Duchemin, A. Thuault, A. Vicente, B. Rigaud, C. Fernandez, S. Eve, Ultrastructure of cellulose crystallites in flax textile fibres, Cellulose 19 (2012) 1837–1854.

[38] M. Kabir, H. Wang, K. Lau, F. Cardona, Effects of chemical treatments on hemp fibre structure, Appl. Surf. Sci. 276 (2013) 13–23.

[39] F. Correia, D. Roy, K. Goel, Chemistry and delignification kinetics of Canadian industrial hemp, J. Wood Chem. Technol. 21 (2001) 97–111.

[40] I.B. Gunnarsson, M. Kuglarz, D. Karakashev, I. Angelidaki, Thermochemical pretreatments for enhancing succinic acid production from industrial hemp (Cannabis sativa L.), Bioresour. Technol. 182 (2015) 58–66.

[41] S.N. Kabekkodu, J. Faber, T. Fawcett, New powder diffraction file (PDF-4) in relational database format: advantages and data-mining capabilities, Acta Crystallogr. Sect. B: Struct. Sci. 58 (2002) 333–337.

[42] S. Amziane, F. Collet, M. Lawrence, C. Magniont, V. Picandet, M. Sonebi, Recommendation of the RILEM TC 236-BBM: characterisation testing of hemp shiv to determine the initial water content, water absorption, dry density, particle size distribution and thermal conductivity, Mater. Struct. 50 (2017) 1–11.

[43] B. Standard, Acoustics-determination of sound absorption coefficient and impedance in impedance tubes—part 2: transfer-function method, BS EN ISO 2001 (2001) 10534-10532.

[44] K.A. Moges, N. Dalila, P. Plaskota, S. Pyo, Evaluation methods, testing standards, and simulation techniques of sound absorption capabilities of cementitious materials: a review, J. Build. Eng. 96 (2024) 110468, https://doi.org/10.1016/j.jobe.2024.110468.

[45] A. Sheppard, S. Latham, J. Middleton, A. Kingston, G. Myers, T. Varslot, A. Fogden, T. Sawkins, R. Cruikshank, M. Saadatfar, Techniques in helical scanning, dynamic imaging and image segmentation for improved quantitative analysis with X-ray micro-CT, Nucl. Instrum. Methods Phys. Res., Sect. B 324 (2014) 49–56.

[46] S. Afroz, Y. Zhang, Q.D. Nguyen, T. Kim, A. Castel, Effect of limestone in general purpose cement on autogenous shrinkage of high strength GGBFS concrete and pastes, Construct. Build Mater. 327 (2022) 126949.

[47] Y.M. Amran, N. Farzadnia, A.A. Ali, Properties and applications of foamed concrete; a review, Construct. Build Mater. 101 (2015) 990–1005.

[48] F.C. McCormick, Ratioanl proportioning of preformed foam cellular concrete, J. Proc. (1967) 104–110.

[49] Z.-L. Jiang, Y.-J. Pan, J.-F. Lu, Y.-C. Wang, Pore structure characterization of cement paste by different experimental methods and its influence on permeability evaluation, Cem. Concr. Res. 159 (2022) 106892.

[50] S. Diamond, Mercury porosimetry: an inappropriate method for the measurement of pore size distributions in cement-based materials, Cem. Concr. Res. 30 (2000) 1517–1525.

[51] H. Giesche, Mercury porosimetry: a general (practical) overview, Part. Part. Syst. Charact. 23 (2006) 9–19.

[52] A. Vishavkarma, H.K. Venkatanarayanan, Assessment of pore structure of foam concrete containing slag for improved durability performance in reinforced concrete applications, J. Build. Eng. 86 (2024) 108939.

[53] H. Moller, C.S. Pedersen, Hearing at low and infrasonic frequencies, Noise Health 6 (2004) 37–57.

[54] S. Nguyen, A. Tran-Le, M. Vu, Q. To, O. Douzane, T. Langlet, Modeling thermal conductivity of hemp insulation material: a multi-scale homogenization approach, Build. Environ. 107 (2016) 127–134.

[55] S.-Y. Chung, J.-S. Kim, D. Stephan, T.-S. Han, Overview of the use of micro-computed tomography (micro-CT) to investigate the relation between the material characteristics and properties of cement-based materials, Construct. Build Mater. 229 (2019) 116843.

[56] N. Bossa, P. Chaurand, J. Vicente, D. Borschneck, C. Levard, O. Aguerre-Chariol, J. Rose, Micro-and nano-X-ray computed-tomography: a step forward in the characterization of the pore network of a leached cement paste, Cem. Concr. Res. 67 (2015) 138–147.

[57] J. Li, A. Hajimohammadi, T. Kim, The surface treatment of PVA fibres to enhance fibre distribution and mechanical properties of foam concrete, Construct. Build Mater. 425 (2024) 136111.

[58] X. Zhao, A.H. Brozena, L. Hu, Critical roles of pores and moisture in sustainable nanocellulose-based super-thermal insulators, Matter 4 (2021) 769–772.

[59] H. Liu, X. Zhao, Thermal conductivity analysis of high porosity structures with open and closed pores, Int. J. Heat Mass Transf. 183 (2022) 122089.

[60] L. Cao, Q. Fu, Y. Si, B. Ding, J. Yu, Porous materials for sound absorption, composites, Communications 10 (2018) 25–35.

[61] R. Del Valle-Zermeño, J.-E. Aubert, A. Laborel-Préneron, J. Formosa, J. Chimenos, Preliminary study of the mechanical and hygrothermal properties of hemp-magnesium phosphate cements, Construct. Build Mater. 105 (2016) 62–68.

[62] P.I. Pelissari, R.A. Angélico, V.R. Salvini, D.O. Vivaldini, V.C. Pandolfelli, Analysis and modeling of the pore size effect on the thermal conductivity of alumina foams for high temperature applications, Ceram. Int. 43 (2017) 13356–13363.

[63] G. Pia, U. Sanna, An intermingled fractal units model to evaluate pore size distribution influence on thermal conductivity values in porous materials, Appl. Therm. Eng. 65 (2014) 330–336.

[64] D.S. Smith, A. Alzina, J. Bourret, B. Nait-Ali, F. Pennec, N. Tessier-Doyen, K. Otsu, H. Matsubara, P. Elser, U.T. Gonzenbach, Thermal conductivity of porous materials, J. Mater. Res. 28 (2013) 2260–2272.

[65] D.S. Smith, S. Fayette, S. Grandjean, C. Martin, R. Telle, T. Tonnessen, Thermal resistance of grain boundaries in alumina ceramics and refractories, J. Am. Ceram. Soc. 86 (2003) 105–111.

[66] M.S. Tuğluca, E. Özdoğru, H. İlcan, E. Özçelikci, H. Ulugöl, M. Şahmaran, Characterization of chemically treated waste wood fiber and its potential application in cementitious composites, Cement Concr. Compos. 137 (2023) 104938.

[67] D. Wanasinghe, F. Aslani, G. Ma, Effect of water to cement ratio, fly ash, and slag on the electromagnetic shielding effectiveness of mortar, Construct. Build Mater. 256 (2020) 119409.

[68] A.H. Mahmood, S.J. Foster, A. Castel, High-density geopolymer concrete for Port Kembla breakwater upgrade, Construct. Build Mater. 262 (2020) 120920.